The University of Reading

School of Mathematical and Physical Sciences

Heat Transfer in a Buried Pipe

Martin Conway

August 2010

This dissertation is a joint MSc in the Departments of Mathematics & Meteorology and is submitted in partial fulfilment of the requirements for the degree of Master of Science

DECLARATION:

I confirm that this is my own work, and the use of all material from other sources has been properly and fully acknowledged.

Signed .....

ACKNOWLEDGEMENTS:

I would like to thank my supervisors Dr. Stepher Langdon and Prof. Mike Baines for their help and advice during the course of this dissertation. I would also like to thank the NERC for their financial support.

Abstract

In this dissertation, we are considering the heat transfer from a pipe buried underground. This is a classic heat diffusion problem which has many applications in the oil and gas industry as well as other agricultural and domestic uses. The simplified problem under consideration in this dissertation concerns an underground pipe with circular cross-section buried in soil which we assume has constant thermal properties. Heat diffuses with a given flux rate across the boundary of the pipe, and at a different flux rate at ground level. We are interested in the temperature distribution below the ground surface, exterior to the pipe when the temperature is in a steady state. Since there is no time dependency, we are effectively solving Laplace's Equation in two dimensions on an exterior domain with Neumann boundary conditions given on the pipe boundary and at the ground surface.

The aim of this dissertation is to derive an accurate numerical solution using Boundary Element Methods. There are several methods we could deploy to solve this equation, depending on the boundary conditions, but we will demonstrate why this method is highly suitable for this particular problem. There will be numerous examples given to demonstrate that an accurate solution has been achieved and we will also highlight techniques which enhance accuracy often for very little extra computational cost. The examples given may not necessarily accurately reflect real world physical situations - rather the aim is to be able to benchmark numerical solutions versus analytic solutions where possible so that we can prove the method to be robust.

In Section 1 we introduce the problem and give some background material, then in Section 2 we formulate the Boundary Integral Equation using Green's Second Identity. In Section 3, we introduce the numerical methods and techniques we will use when solving the Boundary Integral Equation and in Section 4, we give numerical examples to support the theory. In Section 5, we look at the situation where the pipe is only partially buried underground. This requires some adaptation of the previous theory which we will outline. Some further examples are provided to illustrate the robustness of adapted method.

Contents

1 Introduction

1.1 Background

The problem of heat transfer from a buried pipe is a classic heat conduction problem that has many applications in the real world. These applications can be as small-scale as underfloor heating systems such as the Ondol system used in Korea which uses heat generated from cooking stoves [7], to more large scale applications such as oil or gas pipelines either under the seabed or underground. Agriculture has other applications for the consideration of heat transfer of pipes [8]. Soil warming in agriculture is an efficient method of increasing crop yield and growth rates, and can be cost-effective if it uses low energy sources such as industrial waste heat, geothermal or solar energy.

The oil industry clearly has a major interest in the field of heat transfer from buried pipes, and many research companies [13] devote considerable resources trying to model the effects for the large oil and gas companies. One reason for this is that temperature and pressure affect the viscosity of the fluid travelling through the pipeline. This can, in turn, determine the state of the fluid flowing through the pipe (i.e. liquid or gas). Another concern particularly with increasing volumes of oil and gas coming from Arctic regions is the effect of freezing around oil and gas pipes in the vicinity of permafrost [15]. Of importance here is the outward advance of the thaw front around the warm pipe.

In this dissertation, we consider the numerical solution of a simple model of heat transfer from a buried pipe. It is unrealistic to model all the physical factors that could affect the temperature distribution around the pipe. These may include, to name only a few, moisture in the soil, gravitational effects, physical properties due to geological formation around the pipe, and variable heat conductivity throughout the region of interest. Most models make idealised assumptions, such as constant thermal properties of the soil surrounding the pipe, to facilitate a tractable solution. In this dissertation, we therefore consider heat transfer in two dimensions only which effectively looks at a cross-section of the pipe in the ground. The region we are considering is external to the pipe and below ground level. We also assume that the steady-state temperature has been reached so that we can ignore any time dependency; this also implies that the heat flux is constant throughout the region. Despite all these simplifications, the solution can still give a good insight into how heat may be diffused throughout the region.

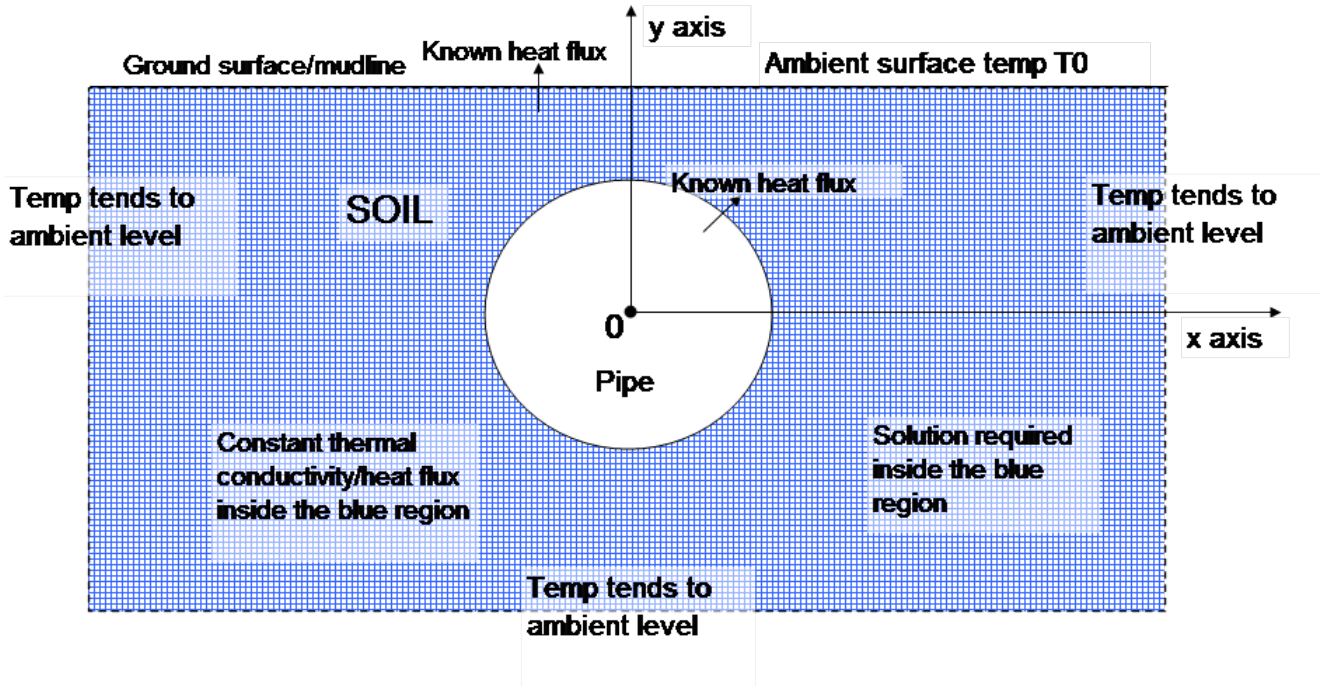

Figure 1: Schematic of the physical situation

1.2 Governing equation

The starting point for our model is derived from Fourier's Law [21] which specifies that heat transfer is governed by the equation:

$$\mathbf{q} = -\kappa \nabla \mathbf{u} \tag{1}$$

where:

$$\begin{aligned} \mathbf{q} &\equiv \text{ heat flux vector per unit length} \\ \kappa &\equiv \text{ heat conductivity of the soil} \\ \mathbf{u} &\equiv \text{ temperature throughout the region.} \end{aligned}$$

If our system is in steady-state, then Conservation of Energy [21] implies that, in the absence of heat sinks or sources, the heat flux throughout the region must satisfy:

$$\nabla \cdot \mathbf{q} = 0. \tag{2}$$

In one dimension, this would imply that heat flux must be constant at all points; in more than one dimension, it implies that heat flux entering a control region must equal heat flux leaving the same region. If we assume that all thermal properties are constant, then κ is constant and (2) reduces to Laplace's Equation:

$$\nabla^2 \mathbf{u} = 0.$$

The simplest scenario for which we can solve this problem analytically is to assume that:

- the pipe is buried deep underground
- the temperature depends only on the distance from the centre of the pipe, O
- the region exterior to the pipe is unbounded.

Under these assumptions, we could now transform Laplace's equation into polar coordinates (r, θ), centred at O, which would yield the solution:

$$u(r) = A \ln r + B$$

where A and B are constants; these can be determined if we know $u(r)$ and $\dfrac{\partial u}{\partial r}$ on the boundary of the pipe $r = a$, where a is the radius of the pipe. This solution blows up as $r \to \infty$ so is only of limited interest in estimating the temperature distribution near the pipe. When the boundary at ground level is introduced, it becomes clear we cannot parametrise the solution by r alone. The purpose of highlighting this solution is that it provides the basis for the Fundamental Solution of Laplace's Equation which we will discuss later in this dissertation (see §2.1).

1.3 Boundary Conditions

In this problem, we have two boundaries of interest which will determine the solution u; the pipe boundary and the ground surface/mudline. There has been much research on modelling the heat transfer associated with buried pipes with constant wall temperatures [7]. A widely used concept here is the conduction shape factor, S, which for a buried pipe takes the form:

$$S = \frac{2\pi}{\cosh^{-1}\left(\frac{Y}{a}\right)}$$

where a is the pipe radius, and Y is the distance of the pipe centre from the ground.
This formulation leads to some unphysical heat transfer properties at the surface when both pipe and surface boundary temperatures are constant. This approach gives better results when the heat flux is given on the ground surface - a more detailed account is given in the paper by Bau and Sadhal [4].

Rather than prescribing the temperature on these boundaries, we are assuming that the heat flux, $\mathbf{q}$ will be known, and hence $\dfrac{\partial u}{\partial n}$ can be prescribed on each boundary. On the pipe boundary, we set $\dfrac{\partial u}{\partial n} = f$ and on the ground surface we set $\dfrac{\partial u}{\partial n} = g$, where f, g are known functions. On the pipe boundary, in terms of polar coordinates $(r, \theta), r$ is fixed so f will depend only on θ; in terms of Cartesian coordinates $(x, y), g$ will depend on x alone since y is fixed so will depend on both r and θ. This type of problem, where we seek a solution u in a region outside a closed domain (i.e. the pipe) and $\dfrac{\partial u}{\partial n}$ is given on the boundary, is known as an exterior Neumann problem.

As we get further away from the heat source of the pipe, we wish the solution to tend towards an ambient temperature. The ambient temperature at the ground surface, T_0, is easy to measure, but as we go further underground it is realistic to expect the temperature to increase. Again this is an idealised condition since in some shallow underground caves the temperature would be much cooler than at the

surface due to lack of sunlight and moisture considerations. However, in some deep mines (4 km underground) in South Africa for example, temperatures have been known to climb to around $55°C$, well above ambient ground temperatures [19]. As a simplification we assume $u \to cy + T_0$ as we get further away from the pipe, where c is a negative constant, $|y|$ is the depth below the centre of the pipe, O. A more mathematically rigorous analysis of this asymptotic behaviour will be given in §2.4.

1.4 Methods of Solution

First, we summarise the exterior Neumann problem we wish to solve:

$$\nabla^2 u = 0 \text{ in D} \tag{3a}$$

$$\frac{\partial u}{\partial n} = f \text{ on } \Gamma_a \tag{3b}$$

$$\frac{\partial u}{\partial n} = g \text{ on } \Gamma_1 \tag{3c}$$

$$u \to cy + T_0 \text{ as } |x| \to \infty, y \to -\infty \tag{3d}$$

where D is the region exterior to the pipe, Γ_a is the pipe boundary, and Γ_1 is the ground surface boundary (for a fuller description see §2.1 and Figure 3).

There are several ways we could go about trying to solve (3). We now describe some of the options available highlighting strengths and weaknesses of each approach, with some illustrative examples where appropriate. At this point we will not be applying full mathematical rigour to any results; this will be done later in §2.4.

1.4.1 Analytic solution using polar coordinates (r, θ)

Generally it is not possible to solve this problem analytically for a general boundary condition at ground level. There are two scenarios where it is possible to have an analytic solution (depending on the nature of the boundary conditions f, g). This is very useful because this gives us a benchmark solution for our numerical model, and gives us an indication of how accurate our solution will be in other scenarios.

The first scenario is when the pipe is buried deep underground and the heat flux at ground level is 0. Thus we can set $g = 0$. We also assume for now that $c = 0, T_0 = 0$ for simplicity. Problem (3) now reduces to:

$$\begin{aligned} \nabla^2 u &= 0 \text{ in D} \\ \frac{\partial u}{\partial n}(a, \theta) &= f(\theta) \text{ on } \Gamma_a. \end{aligned} \tag{4}$$

In summary, this becomes an eigenvalue problem such that there are an infinite number of solutions,

$$\begin{aligned} u_n &= \frac{1}{r}(A_n \cos n\theta + B_n \sin n\theta) \\ u &= \sum_0^\infty u_n \end{aligned} \tag{5}$$

where we have used the fact that u_n must not blow up as $r \to \infty$ and u_n is 2π-periodic. Furthermore,

$$A_n = \frac{a^2}{\pi} \int_0^{2\pi} f(\theta) \cos n\theta d\theta$$
$$B_n = \frac{a^2}{\pi} \int_0^{2\pi} f(\theta) \sin n\theta d\theta. \tag{6}$$

Thus for a simple closed-form solution, we could for example choose f to be $\sin\theta$ or $\cos\theta$ which would leave u with one term only. A solution as an infinite sum could be reduced down to a simpler integral form but this would still require numerical methods to solve and would not be that useful as a benchmark.

The second scenario where we may be able to obtain an analytic solution is when the pipe is exactly half-buried. In this case, our boundary conditions apply along the constant lines $r = a, \theta = \pi, \theta = 2\pi$. Our ability to produce a simple analytical expression depends on the boundary conditions. For example, using the following boundary conditions:

$$f(\theta) = \sin 2\theta$$
$$g(x) = \frac{a^3}{x^3}$$

would yield the closed-form solution, $u = \dfrac{a^3 \sin 2\theta}{2r^2}$, where a is the radius of the pipe. Again, this solution would provide useful benchmarking for our numerical solution.

1.4.2 Finite Difference and Finite Element Methods

The finite differerence (FD) method is often used as a brute force method to solve many Partial Differential Equations (PDEs) as it is often easy to set up and understand [9, pp. 167–187]. A two dimensional regular mesh (N×M grid points) is constructed on the region in which we are looking for a solution, using Cartesian coordinates in this case. At each mesh point (x_i, y_j), we use the discretised version of Laplace's Equation:

$$\frac{(u_{i-1,j} + u_{i+1,j} + u_{i,j-1} + u_{i,j+1} - 4u_{i,j})}{\Delta x \Delta y} = 0$$

where $u_{i,j} \approx u(x_i, y_j), \Delta x = x_{i+1} - x_i, \Delta y = y_{j+1} - y_j$ for a uniform mesh. For a Neumann problem, this requires us to solve a system of equations [N×M]×[N×M], so for 10 x, y nodes each, the linear system to be solved would be 100×100. We can immediately see several problems with this method:

- Since this is an external Neumann problem, the mesh would need to cover a large truncated region meaning either a large number of points leading to long compute time, or a coarse discretisation which would imply a significant error. It would also be difficult to check in the model whether the ambient temperature had been reached as $|x|, |y| \to \infty$.
- The pipe boundary is circular which does not lend itself well to a square mesh. We may need to resort to a more sophisticated finite element approach.
- The error in general would be $O(\Delta x^2)$ which may be unacceptably large.

- Although the matrix above would be sparse (many of the elements would be zero), storing such large data structures could have an adverse effect on computational speeds.

Hence for problem (3), we do not expect the Finite Difference Method to provide an acceptably quick and accurate solution.

1.4.3 Conformal mapping

This technique maps the physical region onto a rectangular domain by using a complex transformation [7]:

$$w = \ln\left(\frac{z - i\sqrt{h^2 - a^2}}{z + i\sqrt{h^2 - a^2}}\right).$$

The transformed boundaries now form the boundary of a rectangle in the complex domain which may be easier to handle using separation of variables, although the boundary conditions are different and may be more difficult to handle. For most problems, however, numerical methods may still be involved so this does not necessarily help us solve the problem.

For a much more detailed discussion, refer to [7].

1.4.4 Bipolar coordinates

There are two standard definitions for bipolar coordinate systems:

- Bipolar coordinates (σ, τ). These are defined in Wikipedia [18] as follows:

$$\begin{aligned} x &= a\frac{\sinh\tau}{\cosh\tau - \cos\sigma} \\ y &= a\frac{\sin\sigma}{\cosh\tau - \cos\sigma} \end{aligned} \tag{7}$$

  where the σ-coordinate of a point P equals the angle F_1PF_2 and the τ-coordinate is given by $\tau = \ln\frac{d_1}{d_2}$, where d_1, d_2 are the distances to the two foci F_1, F_2 located at $(-a, 0)$ and $(+a, 0)$ respectively, as shown in Figure 2.

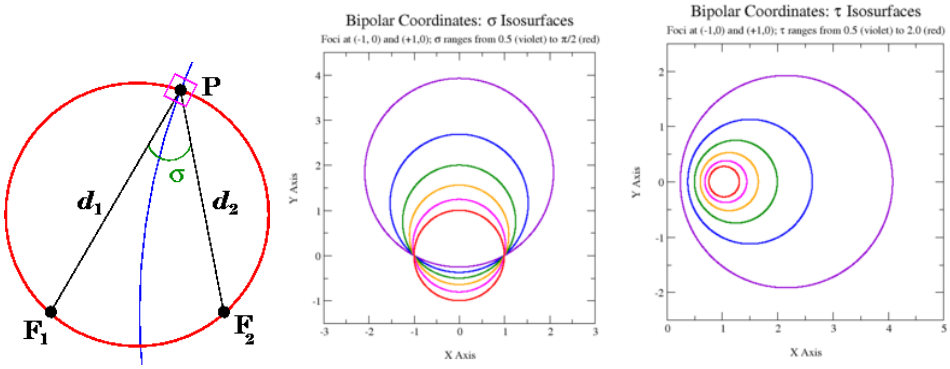

Figure 2: Illustration of bipolar coordinates σ, τ [18]

In (σ, τ) coordinates, $\nabla^2 = \frac{1}{a^2}(\cosh\tau - \cosh\sigma)^2(\frac{\partial^2}{\partial\tau^2} + \frac{\partial^2}{\partial\sigma^2})$.

- Two-centre bipolar coordinates (r_1, r_2) [20]. For a given point $\mathbf{p} = (x, y)$, then r_1 is the distance between $\mathbf{p}$ and the point $(-a, 0)$ and r_2 is the distance between $\mathbf{p}$ and the point $(+a, 0)$.

$$r_1 = \sqrt{(x+a)^2 + y^2}$$
$$r_2 = \sqrt{(x-a)^2 + y^2}.$$

Simple rearrangement yields the transformation to Cartesian coordinates from bipolars (r_1, r_2):

$$x = \frac{r_1^2 - r_2^2}{4a}$$
$$y = \pm\frac{1}{4a}\sqrt{16a^2r_1^2 - (r_1^2 - r_2^2 + 4a^2)^2}. \tag{8}$$

Whilst either of these coordinate systems may be of use solving problem (3), we have not focussed on this method of solution in this dissertation. Elsewhere, analytic solutions have been obtained through this method (see [13],[14]).

1.4.5 Boundary Element Methods

This approach works when the PDE we are looking to solve has a simple Fundamental Solution associated with it. In the case of Laplace's Equation, the Fundamental Solution at a point $\mathbf{p} = (x_p, y_p)$ is:

$$G(x, y|x_p, y_p) = \frac{1}{4\pi}\ln\left[(x - x_p)^2 + (y - y_p)^2\right]. \tag{9}$$

G is defined everywhere in $\mathbb{R}^2$ apart from at (x_p, y_p) where it is singular. As we will see later in §2, we can now transform the PDE (3) into a Boundary Integral Equation (BIE) which we can solve numerically on the boundary of the pipe.

With this approach, there is no need to mesh the semi-infinite domain; we only need to discretise the pipe boundary. In fact we have reduced the dimensionality of the problem from two dimensions to one, as we discretise θ only. When the boundary is smooth as is the case here, we will get rapid convergence as we shall demonstrate in §4. On the downside, we do have to invert dense matrices with this approach, but they tend to be relatively small since we can use a small number of sample points for rapid convergence.

Given the advantages of this approach, we shall now use this method to obtain a solution for (3). There are a couple of different ways this can be done via the Direct Method (which solves for u directly) or the Indirect Method (which solves for a density function which then generates solutions for u). Both these methods are summarised succinctly in [17, 290-297]. We shall use the Direct Method because in this case it has the advantage of immediately yielding the boundary temperature, which we will then use to compute solutions very close to (but not on) the boundary.

2 Formulating the Boundary Integral Equation

2.1 Background

Given the complicated nature of the different domains and boundaries we need to consider, it is helpful to define these in detail for later reference (see Figure 3).

- Let the origin of our Cartesian (x, y) plane, O, be at the centre of the oil pipe.
- Let D_a be the interior of circular pipe radius a, with boundary Γ_a.
- Let the large bounded domain D_{box} be defined by the interior of the region enclosed by the lines $y = Y, x = -R, y = -R, x = +R$.
- Let the boundary of D_{box} be $\Gamma_1, \Gamma_2, \Gamma_3, \Gamma_4$ as shown in the diagram below, where Γ_1 coincides with the line $y = Y$, Γ_2 coincides with the line $x = -R$, Γ_3 coincides with the line $y = -R$, and Γ_4 coincides with the line $x = +R$.
- Define point $\mathbf{p} \in D_{box}/D_a$ and let D_ϵ be a small circular domain, centre $\mathbf{p}$, radius ϵ and boundary Γ_ϵ.
- Let $D = D_{box}/(D_a \cup D_\epsilon)$ with boundary $\Gamma = \Gamma_a \cup \Gamma_\epsilon \cup \Gamma_1 \cup \Gamma_2 \cup \Gamma_3 \cup \Gamma_4$.
- Let G be the Fundamental Solution to Laplace's Equation, $G(\mathbf{p}, \mathbf{q}) = \dfrac{\ln|\mathbf{p} - \mathbf{q}|}{2\pi}$ or in Cartesian terms $G(x_p, y_p | x_q, y_q) = \dfrac{\ln|(x_p - x_q)^2 - (y_p - y_q)^2|}{4\pi}$.
- Let u be the temperature exterior to the pipe, therefore in steady state, u is harmonic on D subject to the boundary conditions $\dfrac{\partial u}{\partial n} = f$ on Γ_a and $\dfrac{\partial u}{\partial n} = g$ on Γ_1. The functions f, g are assumed to be continuously infinitely differentiable i.e $f, g \in C^\infty$.

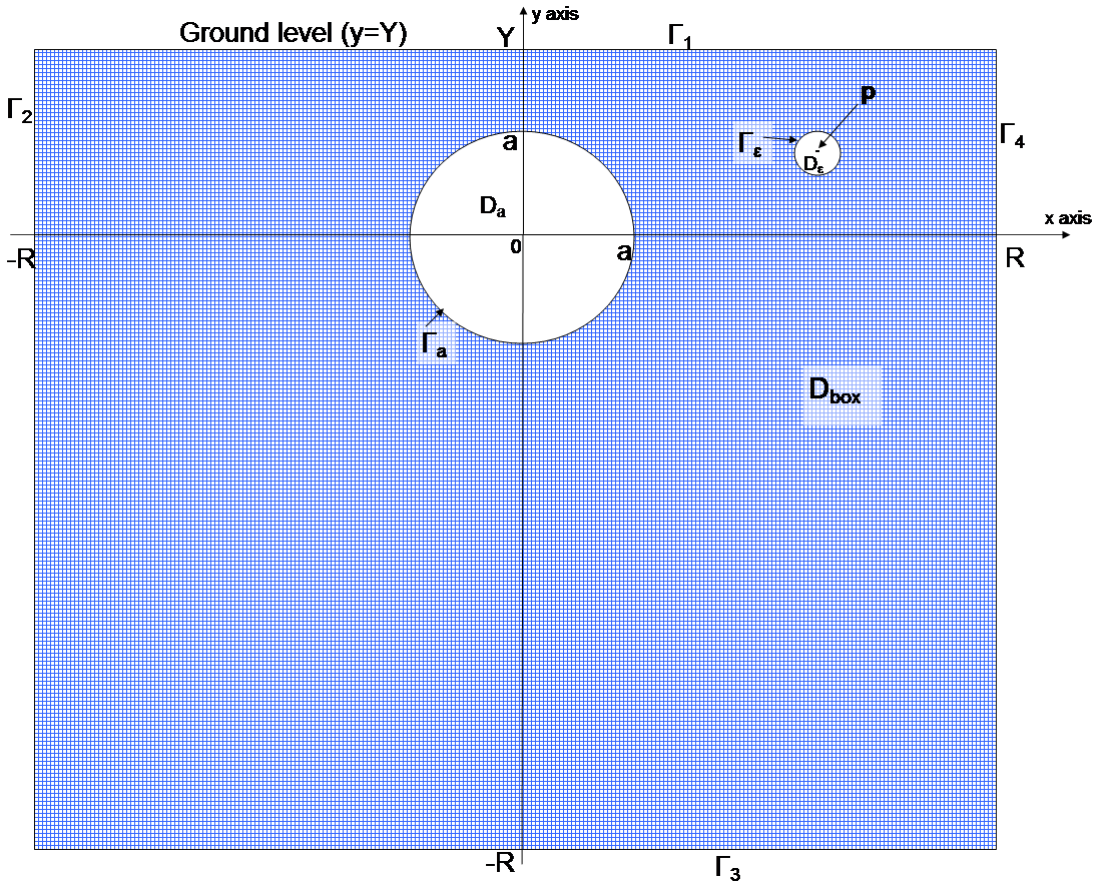

Figure 3: Layout of the different domains and boundaries

To formulate our BIE and to specify constraints on our boundary conditions, we will also need to regularly make use of Green's Second Identity [11, p.69] . This states that if ϕ and ψ are twice continuously differentiable on D in $\mathbb{R}^2$ then:

$$\iint_D (\phi\nabla^2\psi - \psi\nabla^2\phi)dA = \int_\Gamma (\phi\frac{\partial\psi}{\partial n} - \psi\frac{\partial\phi}{\partial n})ds. \tag{10}$$

We define $\dfrac{\partial\phi}{\partial n} = \nabla\phi.\mathbf{n}$ where $\mathbf{n}$ is the unit normal vector pointing out of the domain D, perpendicular to the boundary Γ.

2.2 Assumptions

In order for us to be able to solve Laplace's Equation subject to Neumann boundary conditions, certain constraints need to be imposed to establish existence and uniqueness of solution.

- We assume $u \to cy + T_0$ as $|x|, |y| \to \infty$, where c is some real constant and T_0 is the ambient ground surface temperature. For convenience we therefore introduce a new variable:

$$v = u - cy - T_0 \tag{11}$$

so that $v \to 0$ as $|x|, |y| \to \infty$. v is still harmonic on D and $\dfrac{\partial v}{\partial n} = \dfrac{\partial u}{\partial n} - cn_y$ where n_y is the y component of the outward normal vector to the boundary.

- In order that the solution v does not blow up as $|R| \to \infty$, we need to stipulate that for some real $\alpha > 0$:

$$\begin{aligned} &\frac{\partial v}{\partial x} = O(|x|^{-(1+\alpha)}) \text{ as } |x| \to \infty \\ &\frac{\partial v}{\partial y} = O(|y|^{-(1+\alpha)}) \text{ as } y \to -\infty \\ &v \to 0 \text{ as } |x|, |y| \to \infty, \text{ (which immediately follows from our first assumption).} \end{aligned} \tag{12}$$

  We will see later in §2.4 that this together with compatability (see below) is sufficient to guarantee existence of a unique solution to (3).

- For any harmonic function v in D, substituting $\phi = v$ and $\psi = 1$ into (10), we get:

$$\int_\Gamma \frac{\partial v}{\partial n} ds = 0. \tag{13}$$

  Rewriting boundary conditions for v as $\tilde{f} = f + c\sin\theta$ on Γ_a and $\tilde{g} = g - c$ on Γ_1, then as $R \to \infty$ the integrals over $\Gamma_2, \Gamma_3, \Gamma_4$ disappear and the above condition (13) reduces to:

$$\int_{\Gamma_a} \tilde{f} ds + \int_{\Gamma_1} \tilde{g} ds = 0. \tag{14}$$

  This is known as the **compatability condition**.

  Since $f = \tilde{f} - c\sin\theta$ and $g = \tilde{g} + c$, it follows that we require:

$$\int_{\Gamma_a} f ds + \int_{\Gamma_1} g ds = 0$$

  as all integrals involving the constant c sum to 0.

2.3 Formulation of BIE

To formulate our BIE using the Direct Method, we could make use of (10) by substituting $\phi = v$ and $\psi = G$. Since v and G are harmonic on D, this would give us:

$$\int_\Gamma (v\frac{\partial G}{\partial n} - G\frac{\partial v}{\partial n}) ds = 0 \text{ in D.} \tag{15}$$

Taking each element of Γ in turn, we can see that (15) incorporates values of v on $\Gamma_a, \Gamma_1, \Gamma_\epsilon$ since $\dfrac{\partial G}{\partial n} \neq 0$ on these boundaries. The integrals over $\Gamma_2, \Gamma_3, \Gamma_4$ all disappear as $R \to \infty$ because of our assumptions for v, $\dfrac{\partial v}{\partial n}$ on these boundaries. Solving for v over two distinct boundaries would be cumbersome and also difficult to get an accurate solution since $x \in (-\infty, \infty)$ on Γ_1. Therefore we introduce a modified Green's

function $\tilde{G}$ using method of images such that $\dfrac{\partial \tilde{G}}{\partial n} = 0$ on Γ_1.

The modified Green's function $\tilde{G}$ is defined by:

$$\tilde{G}(x_p, y_p|x_q, y_q) = G(x_p, y_p|x_q, y_q) + G(x_p, y_p|x_q, y_{q'}), \text{ where } y_{q'} = 2Y - y_q. \tag{16}$$

On Γ_1:

$$\frac{\partial \tilde{G}}{\partial n} = \frac{\partial \tilde{G}}{\partial y_q} = \left.\frac{\partial G(x_p, y_p|x_q, y_q)}{\partial y_q}\right|_{y_q = Y} - \left.\frac{\partial G(x_p, y_p|x_q, y_{q'})}{\partial y_{q'}}\right|_{y_{q'} = Y} = 0. \tag{17}$$

$\tilde{G}$ now has two singularities both of which are outside the domain D. Therefore within D, $\tilde{G}$ is still harmonic and so we can still use Green's Second Identity to formulate our BIE.

Using our modified Green's function we can now state that for $\mathbf{p} \in D$:

$$\int_\Gamma \left(v(\mathbf{q}) \frac{\partial \tilde{G}(\mathbf{p}, \mathbf{q})}{\partial n_q} - \tilde{G}(\mathbf{p}, \mathbf{q}) \frac{\partial v(\mathbf{q})}{\partial n_q} \right) ds_q = 0. \tag{18}$$

which will only incorporate values of v on Γ_a and Γ_ϵ since $\dfrac{\partial \tilde{G}}{\partial n} = 0$ on Γ_1. We set out below each element of the above integral and will prove each result in turn.

2.4 Theorems

Theorem 1. *If $\mathbf{p} \in D$ and $\mathbf{q} \in \Gamma_a$, and $\tilde{G}$ is as defined in (16), then for any $\tilde{f} \in C, v$ satisfies:*

$$\int_{\Gamma_a} \left[v(\mathbf{q}) \frac{\partial \tilde{G}(\mathbf{p}, \mathbf{q})}{\partial n_q} - \tilde{G}(\mathbf{p}, \mathbf{q}) \frac{\partial v(\mathbf{q})}{\partial n_q} \right] ds_q = -a \int_0^{2\pi} \left[v(\theta) \left(\frac{\partial \tilde{G}(\mathbf{p}, \mathbf{q})}{\partial x_q} \cos\theta + \frac{\partial \tilde{G}(\mathbf{p}, \mathbf{q})}{\partial y_q} \sin\theta \right) + \tilde{G}(\mathbf{p}, \mathbf{q}) \tilde{f}(\theta) \right] d\theta \tag{19}$$

where $\mathbf{q} = (x_q, y_q) = (a\cos\theta, a\sin\theta)$.

Furthermore, if $\mathbf{p}^* \in \Gamma_a$,

$$\begin{aligned} \int_{\Gamma_a} \left[v(\mathbf{q}) \frac{\partial \tilde{G}}{\partial n_q}(\mathbf{p}^*, \mathbf{q}) - \tilde{G}(\mathbf{p}^*, \mathbf{q}) \frac{\partial v}{\partial n_q}(\mathbf{q}) \right] ds_q = &- \int_0^{2\pi} v(\theta) \left[\frac{1}{4\pi} + a \frac{\partial G}{\partial x_q}(\mathbf{p}', \mathbf{q}) \cos\theta + a \frac{\partial G}{\partial y_q}(\mathbf{p}', \mathbf{q}) \sin\theta \right] d\theta \\ &- \int_0^{2\pi} a \tilde{f}(\theta) \left[\frac{1}{4\pi} \ln\left(4a^2 \sin^2 \frac{(\theta^* - \theta)}{2} \right) + G(\mathbf{p}', \mathbf{q}) \right] d\theta \end{aligned} \tag{20}$$

where $\mathbf{p}^* = (a\cos\theta^*, a\sin\theta^*), \mathbf{p}' = (a\cos\theta^*, 2Y - a\sin\theta^*)$.

Proof. On the left hand side (LHS) of (19), $\dfrac{\partial \tilde{G}}{\partial n_q}$ is defined to be $\nabla \tilde{G}.\mathbf{n_q}$ where n_q is unit normal vector to boundary.
In this case, the **outward** direction is towards the centre of the pipe as this out of the domain D.

Since Γ_a describes a circle, $\mathbf{n_q} = (-\cos\theta, -\sin\theta)$. Therefore $\dfrac{\partial \tilde{G}}{\partial n_q} = -\dfrac{\partial \tilde{G}}{\partial x_q}\cos\theta - \dfrac{\partial \tilde{G}}{\partial y_q}\sin\theta$.
In this case, ds_q describes small changes in arc length, therefore $ds_q = ad\theta$.
Finally we can substitute $\dfrac{\partial v}{\partial n_q} = \tilde{f}$ on Γ_a, leading to equation (19).

To prove equation (20), first observe that for $\mathbf{p} \in \Gamma_a$:

$$\frac{\partial G}{\partial x_q}(\mathbf{p}^*, \mathbf{q}) = \frac{(x_q - x_p)}{2\pi[(x_q - x_p)^2 + (y_q - y_p)^2]}$$

$$\frac{\partial G}{\partial y_q}(\mathbf{p}^*, \mathbf{q}) = \frac{(y_q - y_p)}{2\pi[(x_q - x_p)^2 + (y_q - y_p)^2]}$$

and substitute in the trigonometric expressions for x_p, x_q, y_p, y_q.

This yields:

$$\begin{aligned}\frac{\partial G}{\partial n_q}(\mathbf{p}^*, \mathbf{q}) &= \frac{-a(\cos\theta - \cos\theta^*)\cos\theta - a(\sin\theta - \sin\theta^*)\sin\theta}{2\pi a^2[(\cos\theta - \cos\theta^*)^2 + (\sin\theta - \sin\theta^*)^2]} \\ &= -\frac{(1 - \cos(\theta - \theta^*))}{2\pi a[2 - 2\cos(\theta - \theta^*)]} \\ &= -\frac{1}{4\pi a}. \end{aligned} \tag{21}$$

We also observe that for the reflected Green's function:

$$G(x_p, y_p | x_q, 2Y - y_q) = G(x_p, 2Y - y_p | x_q, y_q) \tag{22}$$

$$\frac{\partial G}{\partial n_q}(x_p, y_p | x_q, 2Y - y_q) = \frac{\partial G}{\partial n_q}(x_p, 2Y - y_p | x_q, y_q). \tag{23}$$

Hence

$$\frac{\partial \tilde{G}}{\partial n_q}(\mathbf{p}^*, \mathbf{q}) = \frac{\partial G}{\partial n_q}(\mathbf{p}^*, \mathbf{q}) + \frac{\partial G}{\partial n_q}(\mathbf{p}^{'}, \mathbf{q}). \tag{24}$$

Using expressions (21) and (24), the first term on the LHS of equation (20) becomes:

$$-\int_0^{2\pi} v(\theta)\left[\frac{1}{4\pi} + a\frac{\partial G}{\partial x_q}(\mathbf{p}^{'}, \mathbf{q})\cos\theta + a\frac{\partial G}{\partial y_q}(\mathbf{p}^{'}, \mathbf{q})\sin\theta\right] d\theta. \tag{25}$$

Now looking at the second term on the LHS of equation (20), we again observe that:

$$\tilde{G}(\mathbf{p}^*, \mathbf{q}) = G(\mathbf{p}^*, \mathbf{q}) + G(\mathbf{p}^{'}, \mathbf{q}). \tag{26}$$

Furthermore,

$$\begin{aligned} G(\mathbf{p}^*, \mathbf{q}) &= \frac{1}{4\pi} \ln \left[a^2(\cos\theta - \cos\theta^*)^2 + a^2(\sin\theta - \sin\theta^*)^2 \right] \\ &= \frac{1}{4\pi} \ln \left[a^2(2 - 2\cos(\theta - \theta^*)) \right] \\ &= \frac{1}{4\pi} \ln \left[4a^2 \sin^2 \frac{(\theta - \theta^*)}{2} \right]. \end{aligned} \tag{27}$$

Substituting (26) and (27) into (20), we obtain the following for the second term on the LHS:

$$-\int_0^{2\pi} a\tilde{f}(\theta) \left[\frac{1}{4\pi} \ln \left(4a^2 \sin^2 \frac{(\theta^* - \theta)}{2} \right) + G(\mathbf{p}', \mathbf{q}) \right] d\theta. \tag{28}$$

Hence our proof is complete for the case where $\mathbf{p}^* \in \Gamma_a$.

□

Theorem 2. *If* **p**,**q**, $\tilde{G}$ *and* Γ_ϵ *are as defined in §2.1–§2.3, then* v *satisfies:*

$$\lim_{\epsilon \to 0} \int_{\Gamma_\epsilon} \left[v(\mathbf{q}) \frac{\partial \tilde{G}(\mathbf{p}, \mathbf{q})}{\partial n_q} - \tilde{G}(\mathbf{p}, \mathbf{q}) \frac{\partial v(\mathbf{q})}{\partial n_q} \right] ds_q = \begin{cases} -v(\mathbf{p}) & \text{if } \mathbf{p} \in D/\Gamma_a \\ -\dfrac{v(\mathbf{p})}{2} & \text{if } \mathbf{p} \in \Gamma_a. \end{cases} \tag{29}$$

Proof. For $\mathbf{p} \in D, \Gamma_\epsilon$ describes a circle, so $\mathbf{p} = (x_p, y_p), \mathbf{q} = (x_p + \epsilon\cos\theta, y_p + \epsilon\sin\theta)$ and $ds_q = \epsilon d\theta$. Hence,

$$\tilde{G} = \frac{1}{4\pi}(2\ln\epsilon + \ln(\epsilon^2 + 2\beta\epsilon\sin\theta + \beta^2)) \text{ where } \beta = 2(Y - y_q) > 0 \tag{30}$$

by substituting above values of x_p, y_p, x_q, y_q into (16).
As $\epsilon \to 0$, it can be seen immediately that the second term in the integral (29) is $O(\epsilon \ln \epsilon)$. Using L'Hôpital's Rule on $\lim_{\epsilon \to 0} \dfrac{\ln \epsilon}{\epsilon^{-1}}$, it can easily be shown that this limit is 0. Therefore we only need to consider the first term.

If $\mathbf{q} \in \Gamma_\epsilon$,

$$\frac{\partial \tilde{G}}{\partial n_q} = -\frac{\partial \tilde{G}}{\partial \epsilon} = -\frac{1}{2\pi\epsilon} - \frac{\epsilon + \beta\sin\theta}{2\pi(\epsilon^2 + 2\beta\epsilon\sin\theta + \beta^2)} \tag{31}$$

by differentiating (30) with respect to ϵ, which gives us:

$$\begin{aligned} \lim_{\epsilon \to 0} \int_{\Gamma_\epsilon} v(\mathbf{q}) \frac{\partial \tilde{G}(\mathbf{p}, \mathbf{q})}{\partial n_q} ds_q &= -\lim_{\epsilon \to 0} \int_0^{2\pi} v(\mathbf{q}) [\frac{1}{2\pi} + \frac{\epsilon(\epsilon + \beta\sin\theta)}{2\pi(\epsilon^2 + 2\beta\epsilon\sin\theta + \beta^2)}] d\theta \\ &= -v(\mathbf{p}). \end{aligned} \tag{32}$$

Now in the case where $\mathbf{p} \in \Gamma_a$, the region D_ϵ is only a segment of a circle depending on ϵ, since D_ϵ must not intersect D_a. As $\epsilon \to 0$, this segment tends towards a semi-circle. Therefore we can repeat the proof as above except we are integrating θ over the range [0,π] instead (see Figure 4).

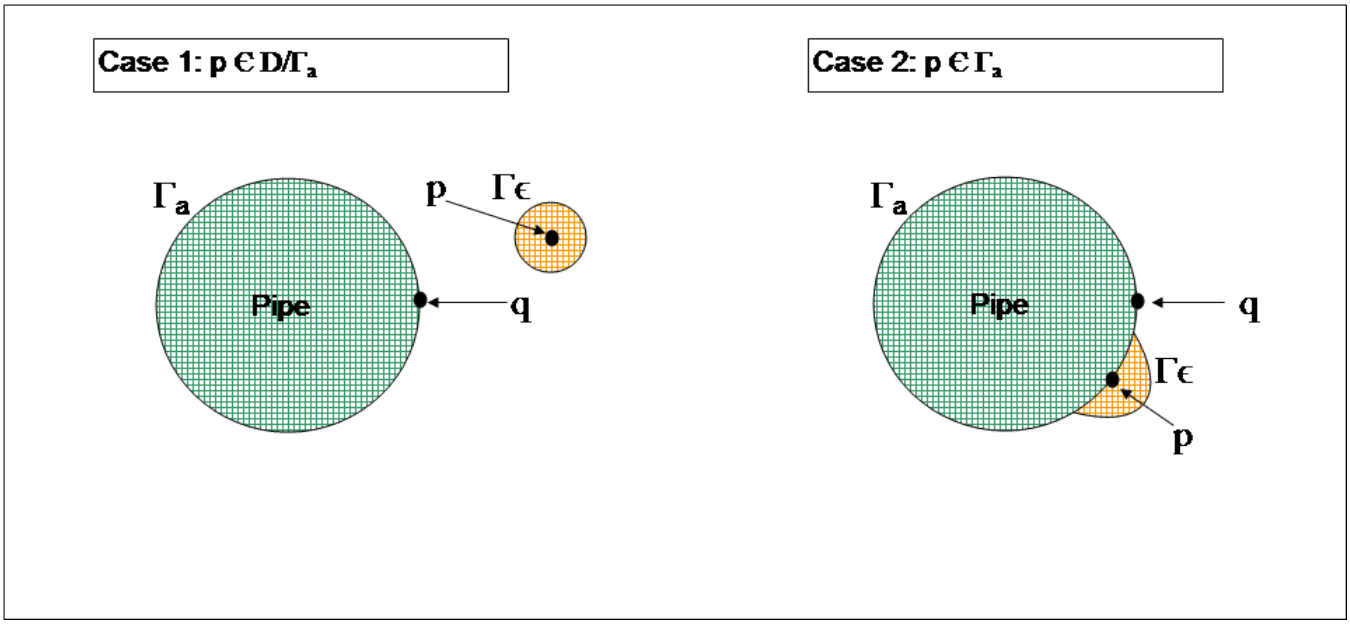

Figure 4: Showing load point **p** in D, and on Γ_a

It follows immediately that:

$$\lim_{\epsilon\to 0}\int_{\Gamma_\epsilon} v(\mathbf{q})\frac{\partial\tilde{G}(\mathbf{p},\mathbf{q})}{\partial n_q}ds_q = -\lim_{\epsilon\to 0}\int_0^\pi v(\mathbf{q})[\frac{1}{2\pi}+\frac{\epsilon(\epsilon+\beta\sin\theta)}{2\pi(\epsilon^2+2\beta\epsilon\sin\theta+\beta^2)}]d\theta$$
$$= -\frac{v(\mathbf{p})}{2}. \tag{33}$$

□

Theorem 3. *If* **p,q**, $\tilde{G}$ *and* Γ_1 *are as defined in §2.1–§2.3, then for any* $\tilde{g}\in C, v$ *satisfies:*

$$\lim_{R\to\infty}\int_{\Gamma_1}[v(\mathbf{q})\frac{\partial\tilde{G}(\mathbf{p},\mathbf{q})}{\partial n_q}-\tilde{G}(\mathbf{p},\mathbf{q})\frac{\partial v(\mathbf{q})}{\partial n_q}]ds_q = -2\int_{-\infty}^{\infty} G(\mathbf{p},\mathbf{q})|_{y_q=Y}\,\tilde{g}(x_q)dx_q. \tag{34}$$

Proof. By definition, on $\Gamma_1, y_q = Y$, $\frac{\partial\tilde{G}}{\partial n_q}=0$, $\frac{\partial v}{\partial n_q}=\tilde{g}$, and $\tilde{G}\Big|_{y_q=Y} = 2\,G|_{y_q=Y}$.
Finally $ds_q = dx_q$ since y_q is constant, hence our result.

□

Theorem 4. *If* **p,q**, $\tilde{G}$ *and* $\Gamma_2,\Gamma_3,\Gamma_4$ *are as defined in §2.1–§2.3, then* v *satisfies:*

$$\lim_{R\to\infty}\int_{\Gamma_i}\left[v(\mathbf{q})\frac{\partial\tilde{G}(\mathbf{p},\mathbf{q})}{\partial n_q}-\tilde{G}(\mathbf{p},\mathbf{q})\frac{\partial v(\mathbf{q})}{\partial n_q}\right]ds_q = 0 \text{ for } i=2,3,4. \tag{35}$$

Proof. First consider the boundary Γ_4 where $x_q = +R$.
Since $\frac{\partial v}{\partial n_q}=\frac{\partial v}{\partial x_q}=O(|x_q|^{-(1+\alpha)})$ as $|x_q|\to\infty$, by definition there exist $x_0, M\in\mathbb{R}$ such that $\frac{\partial v}{\partial x_q}\le Mx_q^{-(1+\alpha)}$ for all $x_q\ge x_0$.

Also since $v \to 0$ as $|x| \to \infty$, there exists $x_1 \in \mathbb{R}$ such that for any $\epsilon > 0, |v| \leq \epsilon$ for all $x \geq x_1$.
Therefore for $R \geq \max(x_0, x_1)$ we can rewrite LHS of (35) as:

$$\begin{aligned}
\left| \int_{-R}^{R} (v\frac{\partial \tilde{G}}{\partial x_q})\Big|_{x_q=R} - (\tilde{G}\frac{\partial v}{\partial x_q})\Big|_{x_q=R} dy_q \right| &\leq \int_{-R}^{R} \left| v(R,y_q)\frac{\partial \tilde{G}}{\partial x_q}(x_p,y_p|R,y_q) \right| dy_q + \int_{-R}^{R} \left| \tilde{G}(x_p,y_p|R,y_q)\frac{\partial v}{\partial x_q}(R,y_q) \right| dy_q \\
&\leq \epsilon \int_{-R}^{R} \left| \frac{\partial \tilde{G}}{\partial x_q}(x_p,y_p|R,y_q) \right| dy_q + MR^{-(1+\alpha)} \int_{-R}^{R} \left| \tilde{G}(x_p,y_p|R,y_q) \right| dy_q \\
&= \frac{\epsilon}{2\pi} \int_{-R}^{R} \left| \frac{(R-x_p)}{(R-x_p)^2+(y_p-y_q)^2} \right| dy_q \\
&\quad + \frac{MR^{-(1+\alpha)}}{4\pi} \int_{-R}^{R} \left| \ln[(R-x_p)^2+(y_q-y_p)^2] \right| dy_q \\
&\leq \frac{\epsilon}{2\pi} \left| \frac{2R}{(R-x_p)} \right| + \frac{MR^{-(1+\alpha)}}{4\pi}.2R\ln(8R^2) \\
&= \frac{\epsilon}{\pi(1-\frac{x_p}{R})} + \frac{(\ln 8 + 2\ln R)MR^{-\alpha}}{2\pi}. \qquad (36)
\end{aligned}$$

As $R \to \infty$ and $\epsilon \to 0$, the first term clearly tends to 0. To prove that $\lim_{R\to\infty} \frac{\ln R}{R^\alpha} = 0$ use L'Hôpital's Rule giving $\lim_{R\to\infty} \frac{\ln R}{R^\alpha} = \frac{1}{\alpha R^\alpha} = 0$.

Hence we have proved that:

$$\lim_{R\to\infty} \int_{\Gamma_4} \left(v(\mathbf{q})\frac{\partial \tilde{G}(\mathbf{p},\mathbf{q})}{\partial n_q} - \tilde{G}(\mathbf{p},\mathbf{q})\frac{\partial v(\mathbf{q})}{\partial n_q} \right) ds_q = 0. \qquad (37)$$

It follows trivially that the same result holds for Γ_2 where we effectively make the substitution $x' = -x$.

We can use the same proof for Γ_3 since we are replacating it using $\frac{\partial v}{\partial y_q}$ as $y_q \to -\infty$ instead of $\frac{\partial v}{\partial x_q}$ as $|x_q| \to \infty$. Although the range of integration [-R,Y] is different, this does not affect the end result. □

We have now proved (35) and are in a position to formulate the BIE to solve this problem.

2.5 The Boundary Integral Equation

2.5.1 Operator Notation

In general, when analysing BIEs, it is convenient to use operator notation to represent integral operators as it is a more compact and convenient notation. It can also be useful when applying rigorous functional analysis techniques to prove existence, uniqueness and to perform error analysis. From a conceptual basis, it is also simple to understand that if the BIE is solved on a particular boundary, we can apply the

same operators (referencing any point in the domain) using those boundary values to solve the equation for that point in the domain.

In this example, we have the following operator representation:

$$v(\mathbf{p}) - (Av)(\mathbf{p}) = (B\tilde{f})(\mathbf{p}) + (C\tilde{g})(\mathbf{p}) \text{ for } \mathbf{p} \in D \tag{38}$$

$$\frac{v(\mathbf{p}^*)}{2} - (Av)(\mathbf{p}^*) = (B\tilde{f})(\mathbf{p}^*) + (C\tilde{g})(\mathbf{p}^*) \text{ for } \mathbf{p}^* \in \Gamma_a \tag{39}$$

where:

$$Az(\mathbf{p}) = \int_{\Gamma_a} z(\mathbf{q}) \frac{\partial \tilde{G}}{\partial n_q}(\mathbf{p}, \mathbf{q}) ds_q$$

$$Bz(\mathbf{p}) = -\int_{\Gamma_a} \tilde{G}(\mathbf{p}, \mathbf{q}) z(\mathbf{q}) ds_q$$

$$Cz(\mathbf{p}) = -\int_{\Gamma_1} \tilde{G}(\mathbf{p}, \mathbf{q}) z(\mathbf{q}) ds_q.$$

2.5.2 Operators on the Boundary

In order to obtain a solution v at any point $\mathbf{p} \in D$, we first need to solve (39) which is a BIE of the Second Kind. Whilst we would use the above definitions of our operators in (38) for a general point $\mathbf{p} \in D$, it is important that we make use of the expressions derived in §2.4 when using the operators in (39). Using these expressions has a significant impact on accuracy and speed when solving the BIE.

The expressions for each operator when $\mathbf{p}^* \in \Gamma_a$ are as follows:

$$Az(\mathbf{p}^*) = -\int_0^{2\pi} z(\theta) \left[\frac{1}{4\pi} + a \frac{\partial G}{\partial x_q}(\mathbf{p}', \mathbf{q}) \cos\theta + a \frac{\partial G}{\partial y_q}(\mathbf{p}', \mathbf{q}) \sin\theta \right] d\theta \tag{40}$$

$$Bz(\mathbf{p}^*) = -\int_0^{2\pi} az(\theta) \left[\frac{1}{4\pi} \ln(4a^2 \sin^2 \frac{\theta^* - \theta}{2}) + G(\mathbf{p}', \mathbf{q}) \right] d\theta \tag{41}$$

$$Cz(\mathbf{p}^*) = -2\int_{-\infty}^{\infty} G(\mathbf{p}^*, \mathbf{q})|_{y_q = Y} \, z(x_q) dx_q. \tag{42}$$

Since the operators B and C do not act on v in our BIE (39) it is convenient to define a function h such that:

$$h(\mathbf{p}^*) = B\tilde{f}(\mathbf{p}^*) + C\tilde{g}(\mathbf{p}^*). \tag{43}$$

The BIE then becomes:

$$\frac{v(\mathbf{p}^*)}{2} - (Av)(\mathbf{p}^*) = h(\mathbf{p}^*) \text{ for } \mathbf{p}^* \in \Gamma_a. \tag{44}$$

Having solved for v on the boundary we can then use (38) to determine v at any point $\mathbf{p} \in D$.

3 Numerical Methods for solving Boundary Integral Equations

3.1 Background

In the previous section, we formulated the BIE which we need to solve on Γ_a. In general, this equation cannot be solved analytically, so we need to develop some numerical techniques to provide the solution. The goal here is to approximate the continuous operators using discrete operators on v so that a linear system of equations on v can then be solved using matrix inversion.

There are several techniques for discretising the BIE; the ones we will look at in this dissertation are known as Nyström's Method and the Collocation Method. Although Galerkin's Method is popular amongst mathematicians due to some of its elegant analytical properties, we will not be discussing it further.

Accuracy in our numerical integration techniques is also critical as this will allow us to use fewer sample points and hence decrease calculation times. Therefore we will be examining different numerical integration rules (known as quadrature), namely the trapezium rule and Gauss-Legendre quadrature, with a view to how precision can be optimised whilst not impacting calculation speeds too adversely.

Finally we will look at some simple examples where the analytic solution is known so we can compare accuracy for the various methods and present some numerical results. This will include examples where the pipe is buried deep underground, and a sequence of results as the pipe approaches ground level.

3.2 Quadrature

Throughout the following discussion, there are numerous references to the term quadrature and the rules used to perform numerical integration. Therefore it would be helpful to set out some definitions here to make the subsequent material clearer.

3.2.1 Definition

A quadrature rule is a numerical approximation for a definite integral, $I = \int_a^b f(x)dx$. In general, an N-point quadrature rule would approximate the integral as:

$$I \approx \sum_{i=1}^{N} w_i f(x_i)$$

where w_i are called the weights and x_i are called the abscissas.
As a simple example, the trapezium rule would approximate the integral as follows:

$$I \approx \frac{(b-a)}{2}(f(a)+f(b))$$

and would therefore be termed a 2-point quadrature rule. Here we have specified the abscissas $x_1 = a, x_2 = b$ and solved for the weights w_1, w_2 to ensure that I is exact when f is any polynomial of order 1 since this gives us two equations in two unknowns.

If the range of integration is subdivided into N equal partitions $[x_i, x_{i+1}]$ where $i = 1, \ldots, N$, we get the composite version of the trapezium rule:

$$\sum_{n=1}^{N} \int_{x_{n-1}}^{x_n} f(x)dx \approx \sum_{n=1}^{N} \frac{(b-a)}{2N}(f(x_{n-1}) + f(x_n)) = \frac{(b-a)}{2N}\left[f(x_0) + f(x_N) + 2\sum_{n=1}^{N-1} f(x_n)\right]. \quad (45)$$

We will see later in §3.7.2 that when the composite trapezium rule is used for smooth periodic functions, we get rapid convergence.

More generally, for an N-point quadrature rule, we can specify N abscissas $x_1, \ldots, x_N$ and calculate the weights $w_1, \ldots, w_N$ accordingly by making sure I is exact when f is any polynomial of order (N-1).

3.2.2 Gauss-Legendre Quadrature

In the above, the abscissas are specified and the weights can be calculated. Gaussian quadrature aims to improve the accuracy by solving simultaneously for both the abscissas and the weights, thereby guaranteeing I is exact for all polynomials of order (2N-1). One of the most popular Gaussian quadrature rules is the Gaussian-Legendre formula, of which we will make widespread use [16, pp. 136–145].

This formula works well when the definite integral is over a finite range [a,b] and the function, $f \in C^\infty$. If there is a singularity in the range, then the quadrature rule can be enhanced to minimise the effect of the singularity and we will examine this later on.

It is customary to use a normalised integration range [-1,1] to calculate the abscissas and weights. They can then be used for any definite integral of any smooth function g. If we can calculate $\{w_i\}, \{x_i\}$ such that:

$$\int_{-1}^{1} f(x)dx \approx \sum_{i=1}^{N} w_i f(x_i), \text{ for any } f \in C^\infty$$

$$\text{then } \int_a^b g(x)dx \approx \frac{(b-a)}{2}\sum_{i=1}^{N} w_i g\left(\frac{b-a}{2}x_i + \frac{b+a}{2}\right) \quad (46)$$

by making the substitution, $x = \frac{b-a}{2}x' + \frac{b+a}{2}$.

It can be shown that the abscissas are the N roots of the Legendre polynomials:

$$P_N(x) = \frac{1}{2^N N!}\frac{d^N}{dx^N}(x^2-1)^N$$

where $P_0(x) = 1, P_1(x) = x, P_2(x) = \frac{1}{2}(3x^2-1), \ldots$.

The weights are then defined as:

$$w_i = \frac{2(1-x_i^2)}{N^2[P_{N-1}(x_i)]^2}.$$

The proof of these results is outside the scope of this document (see [16, pp. 136–145]). However, we will refer to this proof to obtain some properties of the Legendre polynomials needed to calculate the abscissas and weights for any number N.

3.2.3 Calculation of abscissas and weights

The relevant properties we will make use of are:

$$\begin{aligned} P_N(x_i) &= 0 \text{ for } i = 1, 2, ..., N \\ P_N(x) &= \frac{(2N-1)}{N} x P_{N-1}(x) - \frac{(N-1)}{N} P_{N-2}(x) \text{ for all } x \in \mathbb{R}, N \geq 2 \\ P_N^{'}(x) &= \frac{N P_{N-1}(x) - N x P_N(x)}{(1-x^2)} \text{ for all } x \in \mathbb{R}, N \geq 1. \end{aligned} \tag{47}$$

Using a judicious starting value for x_i^0, we will use the recurrence relation in (47) to generate a value for $P_N(x_i^0)$. This value should converge to 0 for x_i to be a root. Therefore we iterate x_i by using the Newton-Raphson method, thereby giving a new start value:

$$x_i^1 = x_i^0 - \frac{P_N(x_i^0)}{P_N^{'}(x_i^0)}.$$

We continue iterating x_i^j in this fashion until $P_N(x_i^j)$ converges towards a given tolerance $\ll 1$. Once this has been achieved, we can then calculate the weight w_i.

The judicious initial guess for x_i can be achieved by using the formula [1, p.787]:

$$x_i = -\cos\frac{(4i+3)\pi}{4N+2}$$

which ensures that there are no repeated roots and that x_i converges to a real root in [-1,1].

We can also save time during the calculation by observing that $P_N(-x) = (-1)^N P_N(x)$ and hence if x_i is a root of $P_N(x)$ then so is $-x_i$. Therefore, for an even number N, we only have to calculate $\frac{N}{2}$ roots and then set $x_i = -x_{N+1-i}$ and $w_i = w_{N+1-i}$ for all $\frac{N}{2} < i \leq N$.

3.2.4 Gaussian quadrature over infinite ranges

As stated previously, Gauss-Legendre is intended for definite integrals over finite ranges with no singularities. In our problem, however, we need to integrate over Γ_1 in which $x_q \in [-\infty, \infty]$. We could employ a different Gaussian quadrature rule such as Gauss-Hermite, but this really needs the integrand f to exhibit exponential decay as $x \to \pm\infty$ for good convergence. There is also the possibility that we need

to split the integral into two semi-infinite ranges to isolate any singularities which would require us to use Gauss-Laguerre quadrature instead. A simpler solution is to transform the infinite (or semi-infinite) range to a finite one by using the substitution:

$$x = \tan\left(\frac{\pi}{2}\lambda\right).$$

Therefore, the integral is now transformed from:

$$\int_{-\infty}^{\infty} f(x)dx \to \frac{\pi}{2}\int_{-1}^{1} f\left(\tan(\frac{\pi}{2}\lambda)\right)\sec^2\left(\frac{\pi}{2}\lambda\right)d\lambda.$$

It can be seen here that we require f to be $O(x^{-(2+p)})$ as $x \to \infty$ (for some $p > 0$) to ensure good convergence, since $\sec^2\left(\frac{\pi}{2}\lambda\right)$ blows up as $\lambda \to \pm 1$. However, this is less onerous than exponential decay and we will explain later how to improve accuracy when the location of a singularity is known. This integral can now be approximated using the standard Gauss-Legendre abscissas and weights.

3.2.5 Gaussian quadrature across a singularity

Using standard Gaussian quadrature where f or its derivatives are singular within the bounds of integration can lead to significant errors being introduced. Sometimes it is possible to make a substitution to get rid of the singularity.

For example,

$$\int_a^b \frac{f(x)}{\sqrt{x}}dx \to \int_{\sqrt{a}}^{\sqrt{b}} \frac{f(y^2)}{y}2ydy$$

by making the substitution, $x = y^2$.

Another technique is to subtract out the singularity by setting $f(x) = f_1(x) + f_2(x)$ where f_1 is relatively smooth and can be numerically integrated more accurately, and f_2 contains the singularity but can be integrated analytically.

For example,

$$\int_0^1 \sin\sqrt{x}dx = \int_0^1 \left(\sin\sqrt{x} - x^{\frac{1}{2}} + \frac{x^{\frac{3}{2}}}{6}\right)dx + \int_0^1 x^{\frac{1}{2}} - \frac{x^{\frac{3}{2}}}{6}dx.$$

The first part of the integral now has first and second derivatives that vanishes at $x = 0$, so can therefore be integrated more accurately. The second part integrates analytically.

Where these two techniques do not help, then we need to refine our Gaussian quadrature to obtain more accuracy. For our problem we shall use a graded one-dimensional mesh.

Suppose the integral is given by:

$$I = \int_0^1 f(x)dx$$

where the singularity is at 0. We then split the integrals into (N+1) ranges such that:

$$I = \int_0^{\sigma^N} f(x)dx + \int_{\sigma^N}^{\sigma^{N-1}} f(x)dx + \int_{\sigma^{N-1}}^{\sigma^{N-2}} f(x)dx + ... + \int_{\sigma}^{1} f(x)dx$$

where $0 < \sigma < 1$. Each of the (N+1) integrals is then approximated numerically using Gauss-Legendre quadrature using N abscissas and weights. The number of calculations is then of order N^2. When using grading in this way it is usual to use a number of weights close to the square root of that used without grading so as to improve accuracy without impairing calculation time.

More generally when integrating over $x \in [a, b]$ with a singularity at a,

$$I = \int_a^{a+(b-a)\sigma^N} f(x)dx + \int_{a+(b-a)\sigma^N}^{a+(b-a)\sigma^{N-1}} f(x)dx + \int_{a+(b-a)\sigma^{N-1}}^{a+(b-a)\sigma^{N-2}} f(x)dx + ... + \int_{a+(b-a)\sigma}^{b} f(x)dx.$$

Similarly, when integrating over $x \in [a, b]$ with a singularity at b,

$$I = \int_{b+(a-b)\sigma^N}^{b} f(x)dx + \int_{b+(a-b)\sigma^{N-1}}^{a+(b-a)\sigma^N} f(x)dx + \int_{b+(a-b)\sigma^{N-2}}^{b+(a-b)\sigma^{N-1}} f(x)dx + ... + \int_{a}^{b+(a-b)\sigma} f(x)dx.$$

Clearly we don't want σ to be too close to 1 otherwise our weighting of the singularity will still produce significant errors. If σ is too close to 0, we will not really have graded the mesh sufficiently since the final integral will dominate. To find the approximate optimal value of σ to be used, we illustrate with an example in Table 1.

Setting $I = -\int_0^{\frac{\pi}{2}} \ln(\sin^2 x)dx$, we tabulate the numerical approximations of I using different values of σ below. In this example, 4 weights were used for each partition. The analytic solution is $I = \pi \ln 2 = 2.177586$ to 6 decimal places, which can be evaluated by comparing the Taylor's expansion of $\ln(1-\cos^2 x)$ and $\ln\left(\frac{1}{2}(1-\cos 2x)\right)$.

σ	I	% error
0.10	2.175232	0.108
0.12	2.176147	0.066
0.14	2.176669	0.042
0.16	2.176967	0.028
0.18	2.177127	0.021
0.20	2.177198	0.018
0.22	2.177205	0.018
0.24	2.177160	0.020
0.26	2.177069	0.024
0.28	2.176936	0.030
0.30	2.176757	0.038

Table 1: Values of I as σ varies from 0.10 to 0.30

This suggests that the optimal value for σ in this scenario would be around 0.20. In practice, when more weights are used an optimal σ of 0.15 is commonly used [12], and this is the value we have used in our examples later on. As a further comparison, when we use 16 weights with no grading, $I = 2.170295$ which gives an error of 0.335%.

3.3 Discretisation Methods

3.3.1 Nyström's Method

Perhaps the simplest discretisation method to understand is Nyström's Method [2, pp. 100–103] which gives a quick and efficient way to discretise BIEs of the Second Kind, using the quadrature rule of our choice to approximate the integral.

In general, suppose we have a BIE such as:

$$v(\mathbf{p}) - Av(\mathbf{p}) = h(\mathbf{p})$$

where $A = \int_\Gamma K(\mathbf{p}, \mathbf{q}) v(\mathbf{q}) ds_q$ and K is a continuous kernel.

We can use a quadrature rule on the operator A such that:

$$(Av)(\mathbf{p}) \approx \sum_{j=1}^{N} w_j K(\mathbf{p}, \mathbf{q_j}) v(\mathbf{q_j})$$

Now suppose that our approximation for v using N node points is v_N, then we can define v_N as follows:

$$v_N(\mathbf{p}) - \sum_{j=1}^{N} w_j K(\mathbf{p}, \mathbf{q_j}) v_N(\mathbf{q_j}) = h(\mathbf{p}) \tag{48}$$

At each node point, p_i where $i = 1, \ldots, N$:

$$v_N(\mathbf{p_i}) - \sum_{j=1}^{N} w_j K(\mathbf{p_i}, \mathbf{q_j}) v_N(\mathbf{q_j}) = h(\mathbf{p_i}) \tag{49}$$

which is a linear system for v_N of order N which can be solved by matrix inversion.

For other points $\mathbf{p} \in D$, we can then write:

$$v_N(\mathbf{p}) = \sum_{j=1}^{N} w_j K(\mathbf{p}, \mathbf{q_j}) v_N(\mathbf{q_j}) + h(\mathbf{p}) \tag{50}$$

Equation (50) is known as Nyström's interpolation formula and is the key to maintaining the accuracy of the solution. This method works well when the kernel K is continuous everywhere and does not contain singularities. In the problem we are looking at however, the kernel of the operator A is the derivative of the Green's function which will become singular for any point $\mathbf{p}$ approaching the boundary Γ_a. In this

instance, to gain greater accuracy we would need to use more points, either by using a larger number of sample points which would be relatively expensive computationally, or by interpolating our solution around the boundary across a larger number of points.

For this reason in our search for greater accuracy close to the pipe boundary, we prefer to use the Collocation Method instead.

3.3.2 Collocation Method

For the collocation method, we first define a finite N-dimensional space of candidate solutions $\{\phi_i\}_{i=1}^N$. The solution for any point $\mathbf{p} \in D \cup \Gamma_a \cup \Gamma_1$ can then be expressed as:

$$v(\mathbf{p}) \approx \sum_{j=1}^{N} c_j \phi_j(\mathbf{p}) \tag{51}$$

and we substitute this into our BIE (44).

Therefore,

$$\begin{aligned}
&\sum_{j=1}^{N} c_j \frac{\phi_j(\mathbf{p})}{2} - A\sum_{j=1}^{N} c_j \phi_j(\mathbf{p}) \approx h(\mathbf{p}) \\
&\sum_{j=1}^{N} c_j \frac{\phi_j(\mathbf{p})}{2} - \sum_{j=1}^{N} c_j A\phi_j(\mathbf{p}) \approx h(\mathbf{p}), \text{ since A is a linear operator} \\
&\sum_{j=1}^{N} c_j \left(\frac{\phi_j(\mathbf{p})}{2} - A\phi_j(\mathbf{p}) \right) \approx h(\mathbf{p}).
\end{aligned} \tag{52}$$

We then chose N collocation points, $\{\mathbf{p_i}\}_{i=1}^N$, on the boundary Γ_a where this equation holds exactly. As there are N collocation points $\{\mathbf{p_i}\}$ and N unknown coefficients $\{c_j\}$, this gives us a system of N linear equations in $\{c_j\}$ which can be solved using matrix inversion.

The matrix representation becomes:

$$\begin{aligned}
\mathbf{Mc} &= \mathbf{h} \\
\mathbf{c} &= \mathbf{M}^{-1}\mathbf{h}
\end{aligned} \tag{53}$$

where:

- M is N×N matrix with elements $M_{ij} = \left(\frac{\phi_j(\mathbf{p_i})}{2} - A\phi_j(\mathbf{p_i}) \right)$
- $\mathbf{c}$ is N×1 vector with elements $\{c_j\}$
- $\mathbf{h}$ is N×1 vector with elements $h(\mathbf{p_i})$.

3.4 Basis functions

The next step in implementing the numerical method is to choose suitable basis functions that we can use in (51). This often depends on factors such as nature of boundary conditions, accuracy required, ease of implementation, speed of computation. Common basis functions include:

- Piecewise constant e.g.

$$\phi_j(x) = \begin{cases} 1 & \text{if } x \in X_j \\ 0 & \text{if } x \notin X_j. \end{cases} \tag{54}$$

  Alternative definitions for X_j are $[x_{j-1}, x_j], [x_j, x_{j+1}]$ or for regularly spaced nodes $[x_j - \frac{\Delta x}{2}, x_j + \frac{\Delta x}{2}]$.

- Piecewise linear e.g.

$$\phi_j(x) = \begin{cases} \dfrac{x - x_{j-1}}{x_j - x_{j-1}} & \text{if } x \in [x_{j-1}, x_j] \\ \dfrac{x_{j+1} - x}{x_{j+1} - x_j} & \text{if } x \in [x_j, x_{j+1}] \\ 0 & \text{otherwise.} \end{cases} \tag{55}$$

- Piecewise polynomial e.g. Lagrange polynomial basis

$$\begin{aligned} \phi_1^N(x) &= \frac{(x-x_0)(x-x_2)(x-x_3)....(x-x_N)}{(x_1-x_0)(x_1-x_2)(x_1-x_3)....(x_1-x_N)} \\ \phi_j^N(x) &= \frac{(x-x_0)(x-x_1)....(x-x_{j-1})(x-x_{j+1})....(x-x_N)}{(x_j-x_0)(x_j-x_1)....(x_j-x_{j-1})(x_j-x_{j+1})....(x_j-x_N)}. \\ \text{Hence } \phi_j^N(x_k) &= \delta_{jk}. \end{aligned} \tag{56}$$

- Trigonometric basis e.g. Lagrange basis functions where 2N points are evenly spaced around a circular boundary [11, p. 182]

$$\phi_j^N(x) = \frac{1}{2N}\left[1 + \cos N(x - x_j) + 2\sum_{n=1}^{N-1} \cos n(x - x_j)\right]. \tag{57}$$

  Lemma 1. *The basis function given in* (57) *has the property that* $\phi_j^N(x_k) = \delta_{jk}$.

  Proof. Consider the case where $j = k$, then trivially $\phi_j^N(x_j) = \frac{1}{2N}\left[1 + 1 + 2\sum_{n=1}^{N-1} 1\right] = 1$.

  For $j \neq k$, first observe that:

$$\cos N(x_k - x_j) = \cos(N(k-j)\frac{2\pi}{N}) = \cos 2\pi(k-j) = 1.$$

Next consider the geometric series:

$$\sum_{n=1}^{N-1} e^{in(x_k - x_j)} = \left(\frac{1 - e^{i(k-j)2\pi}}{1 - e^{\frac{i(k-j)2\pi}{N}}} \right) - 1$$
$$= -1. \tag{58}$$

Therefore, $\frac{1}{2N}\left[1 + \cos N(x_k - x_j) + 2\sum_{n=1}^{N-1} \cos n(x_k - x_j)\right] = 0$ for $j \neq k$.

Hence, $\phi_j^N(x_k) = \delta_{jk}$. □

If we express v in terms of basis functions $\{\phi_j\}_{j=1}^M$ as defined in (57) so that $v(\theta) \approx \sum_{j=1}^{M} \phi_j(\theta) v(\theta_j)$ where $M = 2N$ is an even number, then:

$$Av \approx \int_{\Gamma_a} \frac{\partial G}{\partial n}(\theta) \sum_{j=1}^{M} \phi_j(\theta) v(\theta_j) d\theta \tag{59}$$

$$\approx \sum_{j=1}^{M} v(\theta_j) \left(\int_{\Gamma_a} \frac{\partial G}{\partial n}(\theta) \phi_j(\theta) d\theta \right) \tag{60}$$

If we now use the composite trapezium rule as described in (45) to numerically integrate, we get the following expression:

$$Av \approx \sum_{j=1}^{M} v(\theta_j) \frac{\partial G}{\partial n}(\theta_j) \Delta\theta \tag{61}$$

where $\Delta\theta = \frac{2\pi}{M}$.

This result shows that if our quadrature rule is the composite trapezium rule, and the collocation points are the same as the sample points, then Nyström's Method and the Collocation Method are in fact equivalent.

We shall see in the §3.7.2 that because $\frac{\partial G}{\partial n}(\theta), \phi_j(\theta)$ and every derivative of these functions are all 2π-periodic, then the substitution

$$\int_{\Gamma_a} \frac{\partial G}{\partial n}(\theta) \phi_j(\theta) d\theta = \sum_{j=1}^{M} \frac{\partial G}{\partial n}(\theta_j) \Delta\theta$$

has arbitrarily small error for sufficiently large M.

3.5 Singular Kernels

When calculating $B\tilde{f}$, a problem arises since $\tilde{G}$ has a singularity on Γ_a. Therefore if we were simply to apply the composite Trapezium Rule to numerically integrate we may generate significant errors. However, since the singular kernel in this case is logarithmic, we express $\tilde{f}$ in terms of the Lagrangian

trigonometric basis functions $\{L_j\}$, defined below, to resolve this problem. We can then integrate the resulting interpolation by parts to give us a much more accurate estimate of the integral.

Express $L_j(\theta)$ as a sum of cos terms [11, p.182]:

$$L_j(\theta) = \frac{1}{2N}\left(1 + \cos N(\theta - \theta_j) + 2\sum_{k=1}^{N-1} \cos k(\theta - \theta_j)\right).$$

Let $\tilde{f}(\theta) = \sum_{j=0}^{2N-1} \tilde{f}(\theta_j) L_j(\theta)$ so that $B\tilde{f}(\theta) = \sum_{j=0}^{2N-1} \tilde{f}(\theta_j) B L_j(\theta)$.
The problem arises in trying to calculate

$$w_j(\theta^*) = \int_0^{2\pi} L_j(\theta) \ln\left[4a^2 \sin^2 \frac{(\theta^* - \theta)}{2}\right] d\theta. \tag{62}$$

The integral (62) is a linear sum of integrals where the integrands are all 2π-periodic. Without loss of generality, we can therefore integrate each one over a shifted interval:

$$\int_{\theta^*}^{2\pi+\theta^*} \cos k(\theta - \theta_j) \ln\left[4\sin^2 \frac{(\theta^* - \theta)}{2}\right] d\theta = \int_0^{2\pi} \cos k(\theta - [\theta_j - \theta^*]) \ln\left(4\sin^2 \frac{\theta}{2}\right) d\theta.$$

We now need to prove the following result outlined in [11, p.146], but expanded here for clarity.

Theorem 5.

$$I_k = \int_0^{2\pi} \ln\left(4\sin^2 \frac{\theta}{2}\right) e^{ik\theta} d\theta = \begin{cases} 0 & k = 0 \\ -\frac{2\pi}{|k|} & |k| \geq 1 \end{cases} \tag{63}$$

Proof. When $k = 0$, we observe that:

$$\begin{aligned} I_0 &= \int_0^{2\pi} \ln\left(4\sin^2 \frac{\theta}{2}\right) d\theta \\ &= \int_0^{\pi} \ln\left(4\sin^2 \frac{\theta}{2}\right) d\theta + \int_{\pi}^{2\pi} \ln\left(4\sin^2 \frac{\theta}{2}\right) d\theta \\ &= \int_0^{\pi} \ln\left(4\sin^2 \frac{\theta}{2}\right) d\theta + \int_0^{\pi} \ln\left(4\sin^2 \frac{\phi + \pi}{2}\right) d\phi \\ &= \int_0^{\pi} \ln\left(4\sin^2 \frac{\theta}{2}\right) d\theta + \int_0^{\pi} \ln\left(4\cos^2 \frac{\phi}{2}\right) d\phi \end{aligned} \tag{64}$$

making the substitution $\theta = \phi + \pi$. Similarly,

$$\int_0^{2\pi} \ln\left(4\cos^2 \frac{\theta}{2}\right) d\theta = \int_0^{\pi} \ln\left(4\cos^2 \frac{\theta}{2}\right) d\theta + \int_0^{\pi} \ln\left(4\sin^2 \frac{\phi}{2}\right) d\phi \tag{65}$$

implying that $I_0 = \int_0^{2\pi} \ln\left(4\sin^2 \frac{\theta}{2}\right) d\theta = \int_0^{2\pi} \ln\left(4\cos^2 \frac{\theta}{2}\right) d\theta$.

Therefore,

$$\begin{aligned}
2I_0 &= \int_0^{2\pi} \ln\left(4\sin^2\frac{\theta}{2}\right) + \int_0^{2\pi} \ln\left(4\cos^2\frac{\theta}{2}\right) d\theta \\
&= \int_0^{2\pi} \ln\left(16\sin^2\frac{\theta}{2}\cos^2\frac{\theta}{2}\right) d\theta \\
&= \int_0^{2\pi} \ln\left(4\sin^2\theta\right) d\theta \\
&= \frac{1}{2}\int_0^{4\pi} \ln\left(4\sin^2\frac{\theta}{2}\right) d\theta \\
&= I_0. \qquad (66)
\end{aligned}$$

Hence $I_0 = 0$.

For the case where $k \geq 1$, we need to make use of the geometric sum:

$$\begin{aligned}
1 + e^{ik\theta} + 2\sum_{j=1}^{k-1} e^{ij\theta} &= 1 + e^{ik\theta} + 2\left(\frac{e^{ik\theta}-1}{e^{i\theta}-1} - 1\right) \\
&= (e^{ik\theta}-1)\left\{1 + \frac{2}{e^{i\theta}-1}\right\} \\
&= i(1-e^{ik\theta})\cot\frac{\theta}{2}. \qquad (67)
\end{aligned}$$

Now if we integrate both sides of (67) over [0,2π], we get:

$$2\pi = i\int_0^{2\pi} \cot\frac{\theta}{2}d\theta - i\int_0^{2\pi} e^{ik\theta}\cot\frac{\theta}{2}d\theta. \qquad (68)$$

Using the two identities:

$$\int_0^{\frac{\pi}{2}} \cot\theta d\theta = \int_0^{\frac{\pi}{2}} \tan\theta d\theta$$
$$\int_{\frac{\pi}{2}}^{\pi} \cot\theta d\theta = -\int_0^{\frac{\pi}{2}} \tan\theta d\theta$$

we can easily show that $i\int_0^{2\pi} \cot\frac{\theta}{2}d\theta = 0$.

Therefore (68) now gives us:

$$\int_0^{2\pi} e^{ik\theta}\cot\frac{\theta}{2}d\theta = 2\pi i.$$

Comparing real and imaginary parts, this yields:

$$\int_0^{2\pi} \cos k\theta \cot\frac{\theta}{2} d\theta = 0$$
$$\int_0^{2\pi} \sin k\theta \cot\frac{\theta}{2} d\theta = 2\pi. \tag{69}$$

If we integrate the real part of (63) by parts we obtain:

$$\begin{aligned}\int_0^{2\pi} \ln\left(4\sin^2\frac{\theta}{2}\right)\cos k\theta d\theta &= \left[\ln\left(4\sin^2\frac{\theta}{2}\right)\frac{\sin k\theta}{k}\right]_0^{2\pi} - \frac{1}{k}\int_0^{2\pi} \frac{4\sin\frac{\theta}{2}\cos\frac{\theta}{2}\sin k\theta}{4\sin^2\frac{\theta}{2}} d\theta \\ &= 0 - \frac{1}{k}\int_0^{2\pi} \sin k\theta \cot\frac{\theta}{2} d\theta \\ &= -\frac{2\pi}{k}\end{aligned} \tag{70}$$

using the result (69).

Since I_k is real, then it follows that $I_{-k} = I_k$. Hence for integer values of $k \leq -1$, the value of our integral is $\dfrac{-2\pi}{|k|}$, and our proof is complete. □

Substituting this into (62) we now get:

$$\begin{aligned}w_j(\theta^*) &= \int_0^{2\pi} L_j(\theta+\theta^*)\ln\left[4a^2\sin^2\frac{\theta}{2}\right]d\theta \\ &= \frac{1}{2N}\int_0^{2\pi}\left[\ln a^2 + \ln\left(4\sin^2\frac{\theta}{2}\right)\right]\left[1+\cos N(\theta-\theta_j+\theta^*) + 2\sum_{k=1}^{N-1}\cos k(\theta-\theta_j+\theta^*)\right]d\theta \\ &= \frac{2\pi}{N}\left(\ln a - \left[\sum_{k=1}^{N-1}\frac{1}{k}\cos k(\theta_j-\theta^*) + \frac{1}{2N}\cos N(\theta_j-\theta^*)\right]\right)\end{aligned} \tag{71}$$

by noting that:

$$\begin{aligned}\int_0^{2\pi}\ln\left(4\sin^2\frac{\theta}{2}\right)\cos k(\theta-\theta_j+\theta^*)d\theta &= Re(e^{ik(\theta^*-\theta_j)}I_k) \\ &= -\frac{2\pi}{k}\cos k(\theta_j-\theta^*).\end{aligned} \tag{72}$$

Therefore if operator $B = B_S + B_{NS}$, where B_S is singular and B_{NS} is non-singular, then:

$$(B\tilde{f})(\theta^*) = (B_{NS}\tilde{f})(\theta^*) + \sum_{j=0}^{2N-1} w_j(\theta^*)\tilde{f}(\theta_j).$$

3.6 Numerical integration over an infinite range

When we numerically integrate operator C, we need to integrate across the real line $(-\infty, \infty)$. This integral has no dependency on the integral over the pipe boundary so we can independently choose the optimal way to integrate over Γ_1. The most obvious way is to use the trapezium rule but this produces

poor convergence rates of $O(h^2)$ where $h = R/N$ with R arbitrarily large.

As explained in §3.2, an improvement to this approach would be to use Gaussian quadrature, which for a smooth kernel would be extremely accurate for relatively few points ($N \approx 32$) - Gauss-Hermite would probably give rapid convergence here. However, the kernel becomes singular as the load point approaches the line $y = Y$, which is a problem when we want to solve for all points in the domain D. Gauss-Hermite quadrature also performs best when the integrand decays exponentially as $|x| \to \infty$ which may not be the case in this problem.

An alternative approach is to make a substitution in the integral to give us finite limits so we can then use Gauss-Legendre quadrature. For example, we can choose $x = \tan(\phi)$. Thus the range for ϕ is $(-\frac{\pi}{2}, \frac{\pi}{2})$. This substitution effectively gives us a large Δx as x approaches $\pm\infty$ where we know the solution decays to 0, and a much smaller Δx near $x = 0$ where we need a much more granular discretisation. There are some limitations to using this quadrature which we have stated previously, but in the examples we have used this produces the best convergence.

The equation for operator C now becomes:

$$Cz(\mathbf{p}^*) = -2 \int_{-\frac{\pi}{2}}^{\frac{\pi}{2}} G(\mathbf{p}^*, \mathbf{q}(\phi))|_{y_q=Y} \, z(\phi) \sec^2 \phi d\phi. \tag{73}$$

This kernel is not singular for $\mathbf{p}^* \in \Gamma_a$ if $Y > a$. However, we still have the problem of near singularity for those points $\mathbf{p} \in D$ as $\mathbf{p}$ approaches Γ_1. An improvement is achieved by splitting the integral into two domains (-∞, x_p) and (x_p, ∞), and using the substitutions $x = x_p - \tan\phi$ on the first domain, and use $x = x_p + \tan\phi$ on the second domain. This ensures that the point of singularity (i.e. $x = x_p$) is the upper boundary on the first integral and the lower boundary on the second integral.

We can then use Gauss-Legendre quadrature as described above on both integrals with grading if necessary. The operator C is then transformed to:

$$Cz(\mathbf{p}^*) = -\frac{1}{2\pi} \int_0^{\frac{\pi}{2}} \ln\left[\tan^2(\theta) + (Y - y_p)^2\right] \left[z(x_p + \tan\phi) + z(x_p - \tan\phi)\right] \sec^2 \phi d\phi \tag{74}$$

Given that we have a finite range, we generally use Gauss-Legendre integration with 64 points or with grading we use 8 points on 8 graded domains. This approach shows distinctly better convergence when $\mathbf{p}$ approaches the line $y = Y$ over other traditional approximations such as trapezium rule with $x = \tan\phi$ substitution.

3.7 Error Analysis

We now examine the error for these composite rules to see what order of magnitude we should expect for a given discretisation. This will then give us some basis on which rule to choose for our numerical integration given other considerations such as speed and memory constraints.

3.7.1 Trapezium Rule

We expand the derivation given in Kress for clarity [11, p.198].

Theorem 6. *Let the remainder R(f) be defined as:*

$$R(f) = \int_a^b f(x)dx - h\left[\frac{f(x_0)}{2} + f(x_1) + ... + f(x_{N-1}) + \frac{f(x_N)}{2}\right]. \tag{75}$$

Then $|R(f)| \leq \frac{h^2}{12}(b-a)\left\|f^{''}\right\|_\infty$.

Proof. Define $K(x)$ for each partition of the interval [a,b].

$$K(x) = \begin{cases} \frac{1}{2}(x-x_0)(x-x_1) & x_0 \leq x \leq x_1 \\ .... & \\ \frac{1}{2}(x-x_{j-1})(x-x_j) & x_{j-1} \leq x \leq x_j \\ .... & \\ \frac{1}{2}(x-x_{N-1})(x-x_N) & x_{N-1} \leq x \leq x_N \end{cases} \tag{76}$$

We integrate by parts twice to obtain:

$$\begin{aligned} \int_{x_{j-1}}^{x_j} K(x)f^{''}(x)dx &= \left[\frac{y(y-h)}{2}f^{'}(y+x_{j-1})\right]_0^h - \int_0^h (y-\frac{h}{2})f^{'}(y+x_{j-1}) \\ &= 0 - \left[(y-\frac{h}{2})f(y+x_{j-1})\right]_0^h + \int_0^h f(y+x_{j-1})dy \\ &= -\frac{h}{2}\left[f(x_{j-1}) + f(x_j)\right] + \int_0^h f(y+x_{j-1})dy \\ &= \int_{x_{j-1}}^{x_j} f(x)dx - \frac{h}{2}\left[f(x_{j-1}) + f(x_j)\right]. \end{aligned} \tag{77}$$

Summing over $j = 1, \ldots, N$ we get:

$$\begin{aligned} |R(f)| &\leq \sum_{j=1}^N \int_{x_{j-1}}^{x_j} \left|K(x)f^{''}(x)\right| dx \\ &\leq \left\|f^{''}\right\|_\infty \sum_{j=1}^N \int_0^h |\frac{y(y-h)}{2}|dy \\ &= \left\|f^{''}\right\|_\infty \sum_{j=1}^N \left[\frac{hy^2}{4} - \frac{y^3}{6}\right]_0^h \\ &= \left\|f^{''}\right\|_\infty \frac{Nh^3}{12} \\ &= \frac{h^2}{12}(b-a)\left\|f^{''}\right\|_\infty. \end{aligned} \tag{78}$$

□

3.7.2 Trapezium Rule on Periodic Functions

In the problem we are looking at, we know that our integrand is 2π-periodic around the pipe boundary. Therefore we can use a special feature of the trapezium rule which improves our accuracy from $O(h^2)$ considerably [10].
The most convenient way to analyse the periodicity is to look at the discrete Fourier transform of the integrand f.

$$f(x) = \frac{1}{2\pi} \sum_{m=-\infty}^{\infty} c_m e^{imx}$$

where

$$c_m = \int_0^{2\pi} f(x) e^{-imx} dx.$$

Define the exact integral $I = \int_0^{2\pi} f(x)dx$. It follows immediately that $I = c_0$.
Also define the numerical integral :

$$\begin{aligned} I_N &= \sum_{n=1}^{N} f(n\Delta x)\Delta x \\ &= \sum_{n=1}^{N} (\sum_{m=-\infty}^{\infty} \frac{1}{2\pi} c_m e^{imn\Delta x})\Delta x \\ &= \sum_{m=-\infty}^{\infty} c_m (\sum_{n=1}^{N} e^{\frac{2\pi imn}{N}}) \frac{1}{N}. \end{aligned} \tag{79}$$

But $\sum_{n=1}^{N} e^{\frac{2\pi imn}{N}} = 0$ unless m is an integer multiple of N. So we can simplify the above to:

$$I_N = \sum_{k=-\infty}^{\infty} c_{kN}.$$

Therefore the error in the trapezium rule is:

$$\begin{aligned} E &= |I - I_N| \\ &= \left| c_0 - \sum_{k=-\infty}^{\infty} c_{kN} \right| \\ &= \left| \sum_{k=1}^{\infty} (c_{kN} + c_{-kN}) \right| \\ &= \left| \sum_{k=1}^{\infty} 2 \int_0^{2\pi} f(x) \cos(kNx) dx \right|. \end{aligned} \tag{80}$$

Thus we can see that the error in our trapezium rule approximation is dependent on the discrete Fourier transform of f. In fact there exists N such that the error in the trapezium rule approximation is arbi-

trarily small, since standard Fourier analysis tells us that the coefficients c_m are of order $O(\frac{1}{m^{p+1}})$ for a p-times differentiable function. However, for a function f whose derivatives are all periodic, there may exist values of N where the error is significant.

For example, $f(x) = \cos^5 x$, has a discrete Fourier transform:

$$f(x) = \frac{1}{2\pi} \sum_{m=-5}^{5} c_m e^{imx}$$

where $c_{\pm 5} = \frac{\pi}{16}, c_{\pm 3} = \frac{5\pi}{16}, c_{\pm 1} = \frac{5\pi}{8}, c_m = 0$ otherwise. Since $c_0 = 0$ the exact value of the integral should be 0. From (80) we can see that if we use $N = 1, 3, 5$ we will get errors $2\pi, \frac{5\pi}{8}, \frac{\pi}{8}$ respectively and zero error for other values of N. Thus predicting a value for N which will give an arbitrarily small error for a general function f, is difficult to do analytically and will in all likelihood involve some trial and error.

Alternatively, by using repeated integration by parts on (80), we get the result that:

$$\begin{aligned}\int_0^{2\pi} f(x)\cos(kNx)dx = &\frac{1}{(kN)^2}\left[f^{'}(2\pi) - f^{'}(0)\right] - \frac{1}{(kN)^4}\left[f^{'''}(2\pi) - f^{'''}(0)\right] + ... \\ &+ \frac{(-1)^{p-1}}{(kN)^{2p}}\left[f^{2p-1}(2\pi) - f^{2p-1}(0)\right] + ...\end{aligned}$$

This result is formalised in the Euler Maclaurin Summation Formula [5]. This states that if $f \in C^{2p+2}[0, 2\pi]$ for $p \geq 1$, and I_N is the trapezoidal rule approximation to $\int_0^{2\pi} f(x)dx$ with N uniform subintervals, then:

$$\begin{aligned}E_N &= I_N - I \\ &= \sum_{m=1}^{p} \left(\frac{2\pi}{N}\right)^{2m} \frac{B_{2m}}{(2m)!}\left[f^{2m-1}(2\pi) - f^{2m-1}(0)\right] \\ &+ 2\pi\left(\frac{2\pi}{N}\right)^{2p+2} \frac{B_{2p+2}}{(2p+2)!} f^{2p+2}(\xi). \qquad (81)\end{aligned}$$

where $0 \leq \xi \leq 2\pi$ and B_n is the n^{th} Bernoulli number. This suggests that if f is (2p+2)-times differentiable, and all derivatives are periodic then the error is of order $O(1/N^{2p+2})$ i.e. if $f \in C^{\infty}$ then the error is exponentially small with respect to N.

4 Numerical Examples for a buried pipe

4.1 Exterior Neumann problem on an unbounded domain

4.1.1 Analytic Solution

In order to test our methodology outlined above, and to examine the accuracy of our numerical implementation, it is usual to benchmark using a simple example where the anaytical result is known. Since we know with 100% confidence the true result we can therefore draw conclusions from our numerical approach.

The first example we will look at is solving Laplace's equation with Neumann boundary conditions on an unbounded exterior domain, where the boundary is the rim of the pipe of unit radius. In physical terms, this means that the pipe is deep underground (we set Y = 100,000) and we set $a = 1, c = 0, \tilde{g} = 0$. In order to satisfy the compatability condition, from (14), we must ensure that $\int_{\Gamma_a} \tilde{f} = 0$. Choosing $\tilde{f} = \frac{x}{\sqrt{x^2+y^2}}$ in Cartesian terms, satisfies this condition and makes the problem solvable analytically. We have also stipulated earlier that $v \to 0$ as $|x|, |y| \to \infty$.
If we now transform this problem into polar coordinates (r, θ) then:

$$\begin{aligned} r^2 v_{rr} + r v_r + v_{\theta\theta} &= 0 \\ \frac{\partial v}{\partial r}(a, \theta) &= -\cos\theta \\ \lim_{r\to\infty} v(r, \theta) &= 0. \end{aligned} \tag{82}$$

Using separation of variables $v(r, \theta) = R(r)\Theta(\theta)$, we obtain:

$$\begin{aligned} \frac{r^2 R'' + rR'}{R} &= \lambda \\ \frac{\Theta''}{\Theta} &= -\lambda \end{aligned} \tag{83}$$

where λ is a real constant.

Since v is 2π periodic, so is Θ, and therefore λ must be a positive constant to give a solution of the form $A\cos\sqrt{\lambda}\theta + B\sin\sqrt{\lambda}\theta$. Moreover to satisfy periodicity, $\lambda = n^2$ where n is an integer.

To solve for R in the form $Cr^m + Dr^{-m}$, we must first solve the resulting characteristic equation:

$$\begin{aligned} m(m-1) + m - n^2 &= 0 \\ m &= \pm n. \end{aligned} \tag{84}$$

Given (82), m cannot be positive since the solution would blow up as $r \to \infty$. This gives us a general solution of:

$$v(r, \theta) = r^{-n}(A_n \cos n\theta + B_n \sin n\theta), \text{ where } n \text{ is a positive integer.} \tag{85}$$

Applying boundary conditions from (82), we finally we obtain the solution:

$$v(r, \theta) = \frac{a^2 \cos\theta}{r}. \tag{86}$$

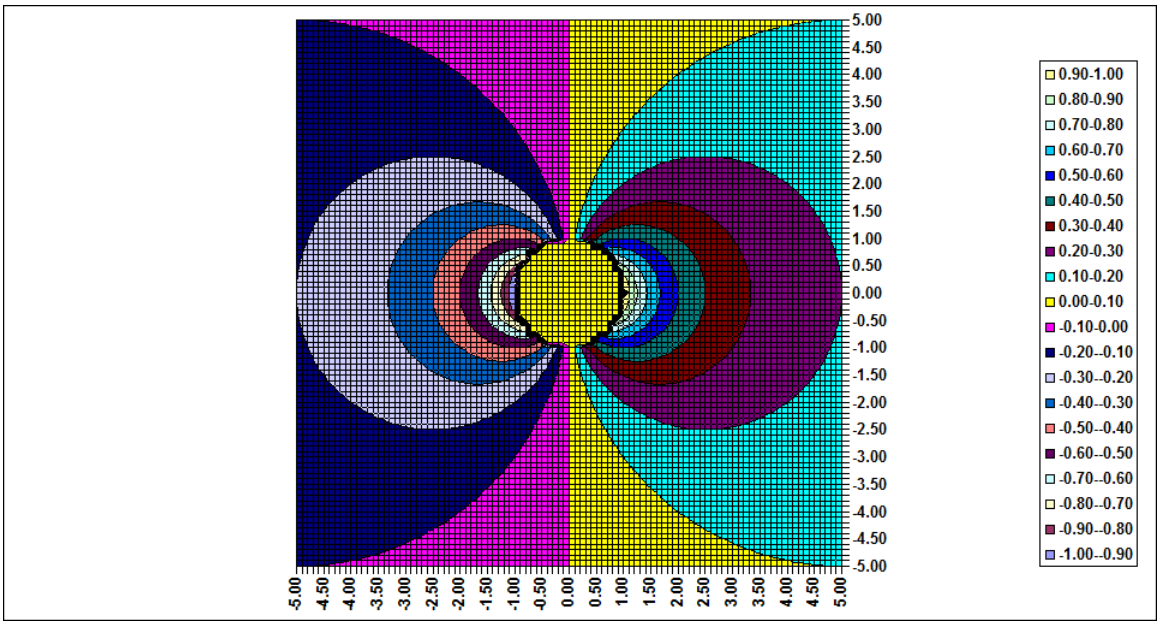

Figure 5: Analytic solution over a square subset of the domain D [-5,5]×[-5,5]

4.1.2 Numerical Solution

We now need to compare this analytic solution to that obtained when we solve using the BIE (44).

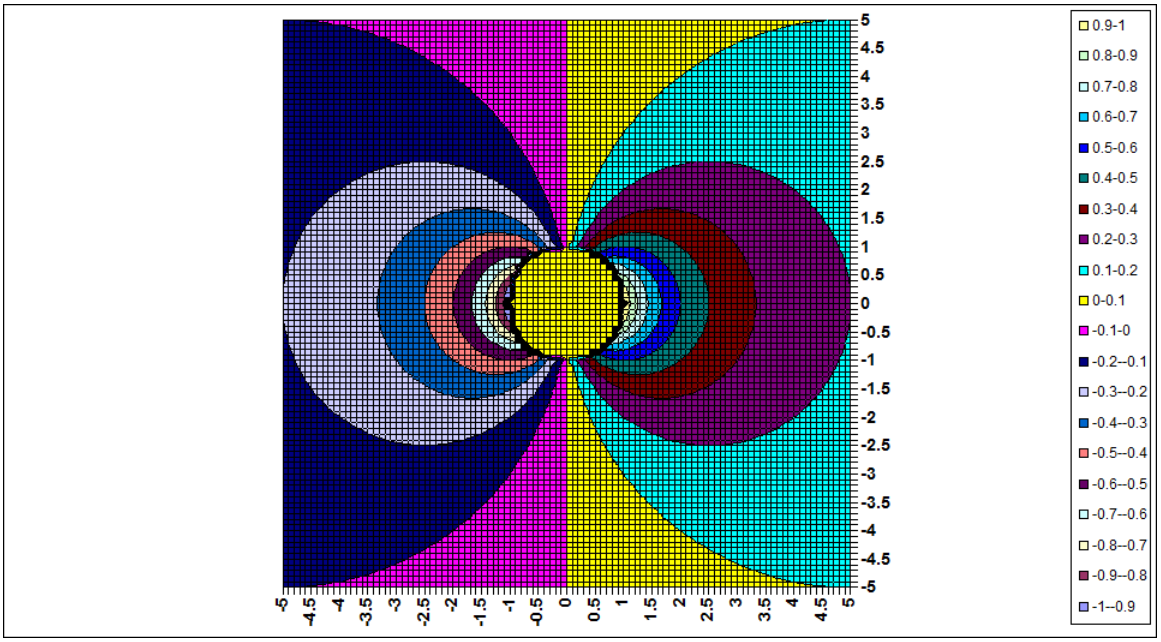

Figure 6: Numerical solution over a square subset of the domain D [-5,5]×[-5,5]

We have used the Lagrange trigonometric basis functions as defined in (57) for v and $\tilde{f}$ and numerically

integrated using the composite trapezium rule. As demonstrated above, since the integrands are 2π-periodic, this should give us extremely fast convergence for relatively small M; in this example we are using $M = 64$. We notice that the analytic and numeric solutions in Figures 5 and 6 look very similar.

4.1.3 Global Error Observations

Although the two graphs at first glance look very alike, there are some significant errors near the pipe boundary which the graph below highlights. This is to be expected since there is a discontinuity in the solution when $\mathbf{p} \in \Gamma_a$. This is a feature of the Green's function only being integrated over a semi-circle to keep within the domain D, rather than over a full circle when the point is inside D.

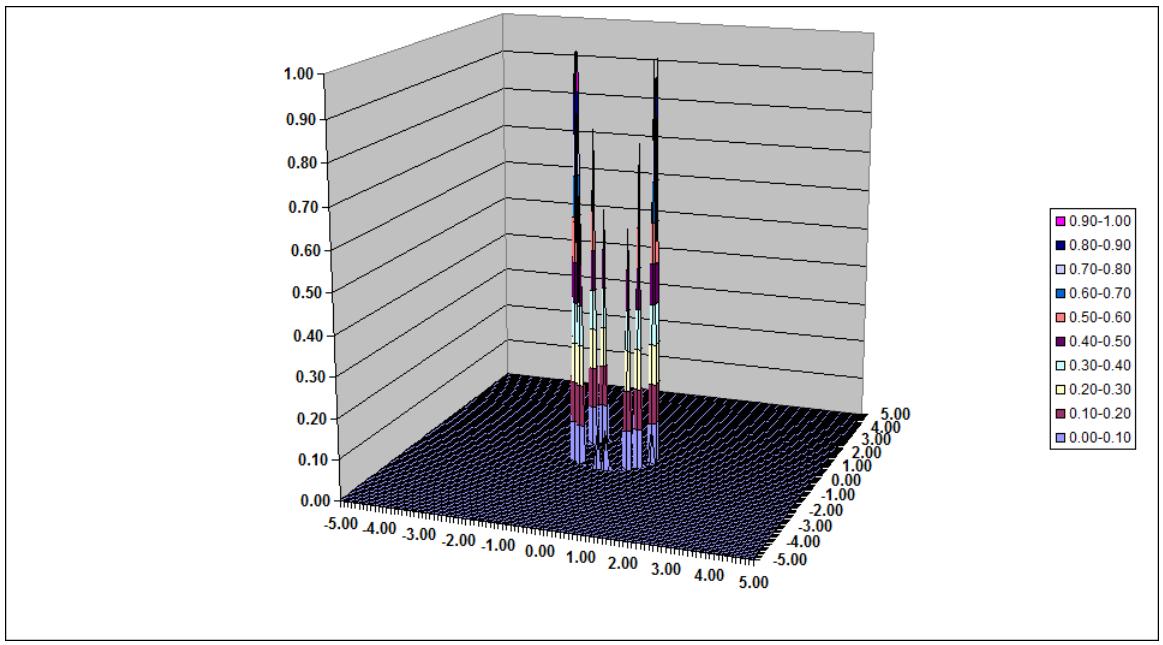

Figure 7: Graph of absolute errors - difference between analytic and numerical solutions

There are several ways we can try to minimise this error:

- **Sample Points**
  Increase the number of sample points on the boundary Γ_a. This is a sledgehammer approach since we only need to increase granularity when $\mathbf{p}$ is approaching the boundary. When $\mathbf{p}$ is sufficiently far away a small number of sample points is perfectly adequate as the graph shows.

- **Collocation Points**
  Increase the number of collocation points used in the numerical integration when $\mathbf{p}$ is sufficiently close to Γ_a. This is possible because we have expressed the solution in terms of Lagrange trigonometric basis functions. These allow us to interpolate any value of v around the boundary Γ_a even though we have only explicitly calculated N values from the BIE. However, each basis function is usually expressed as a sum of $\frac{M}{2}$ trigonometric terms which would require $\frac{M^2}{2}$ calculations to interpolate v. Happily we can reduce the summation of each basis function to one term, meaning

each interpolation only requires M calculations.

From (57) using $M = 2N$,

$$\begin{aligned}
\phi_j^N(x) &= \frac{1}{2N}\left[1 + \cos N(x - x_j) + 2\sum_{n=1}^{N-1}\cos n(x - x_j)\right] \\
&= Re\left\{\frac{1}{2N}\left[1 + e^{iN(x-x_j)} + 2\sum_{n=1}^{N-1} e^{in(x-x_j)}\right]\right\} \\
&= Re\left\{\frac{1}{2N}\left[2\frac{(e^{iN(x-x_j)} - 1)}{(e^{i(x-x_j)} - 1)} + (e^{iN(x-x_j)} - 1)\right]\right\} \\
&= Re\left\{\frac{1}{2N}\left[(e^{iN(x-x_j)} - 1)\frac{(e^{i(x-x_j)} + 1)}{(e^{i(x-x_j)} - 1)}\right]\right\} \\
&= \frac{1}{2N}\sin N(x - x_j)\cot\left(\frac{x - x_j}{2}\right). \qquad (87)
\end{aligned}$$

So if M is the number of sample points $\{x_j\}$ and $v(x_j)$ is the solution we have solved for numerically at these points, then:

$$v(x) = \frac{1}{M}\sum_{j=1}^{M} v(x_j)\sin\frac{M(x - x_j)}{2}\cot\left(\frac{x - x_j}{2}\right). \qquad (88)$$

We can therefore interpolate as much as we want to get better resolution near the boundary, however the disadvantage is slow calculation speeds. For points extremely close to the boundary we can use a quicker, equally accurate approach.

- **Taylor's expansion**
  In this Neumann problem, since we know the normal derivative on the boundary we can use this in the Taylor's expansion of $v(\theta + \Delta\theta)$ to estimate our solution. Suppose ϵ is the radial distance between $\mathbf{p}$ and Γ_a. In this problem:

$$\epsilon = \sqrt{x_p^2 + y_p^2} - a.$$

Therefore expanding we get:

$$\begin{aligned}
v(r + \epsilon, \theta) &\approx v(a, \theta) + \epsilon \left.\frac{\partial v}{\partial r}\right|_{r=a} \\
&= v(a, \theta) - \epsilon\tilde{f}(\theta). \qquad (89)
\end{aligned}$$

Obviously the error term in the approximation here is of $O(\epsilon^2)$ so we need to choose ϵ to give us the precision that we require. However we can improve accuracy by another order by using the fact that Laplace's Equation holds for the point $\mathbf{p}$ near the boundary.
From (82), in polar coordinates we get:

$$v_{rr} = -\frac{1}{r}\frac{\partial v}{\partial r} - \frac{1}{r^2}v_{\theta\theta}.$$

We can therefore estimate v_{rr} at $r = a$ by using boundary data and estimating $v_{\theta\theta}$ with the three point approximation,

$$v_{\theta\theta} = \frac{v(\theta + \Delta\theta) + v(\theta - \Delta\theta) - 2v(\theta)}{\Delta\theta^2}$$

where $\Delta\theta$ can be arbitrarily small and the values of v found by Lagrangian interpolation. This now gives us:

$$v_{rr}|_{r=a} = \frac{1}{a}\tilde{f}(\theta) - \frac{v(a, \theta + \Delta\theta) + v(a, \theta - \Delta\theta) - 2v(a, \theta)}{a^2\Delta\theta^2}.$$

Our new estimate for v becomes:

$$v(r, \theta) = v(a, \theta) - \epsilon\tilde{f}(\theta) + \frac{\epsilon^2}{2}\left(\frac{1}{a}\tilde{f}(\theta) - \frac{v(a, \theta + \Delta\theta) + v(a, \theta - \Delta\theta) - 2v(a, \theta)}{a^2\Delta\theta^2}\right).$$

The error in the approximation is now $O(\epsilon^3)$.

The graph below shows the global error versus the analytic solution from the first example with these refinements to the solution near the boundary.
In this run, we have used:

- Number of sample points on the boundary, $M = 64$
- 320 collocation points when $\frac{a}{20} \leq \epsilon \leq \frac{a}{10}$
- Taylor's expansion to second order when $0 \leq \epsilon \leq \frac{a}{20}$.

We can see that the maximum error has reduced by a factor of around 500 in the vicinity of the boundary so that although the calculation time is considerably longer, the improved accuracy makes this worthwhile.

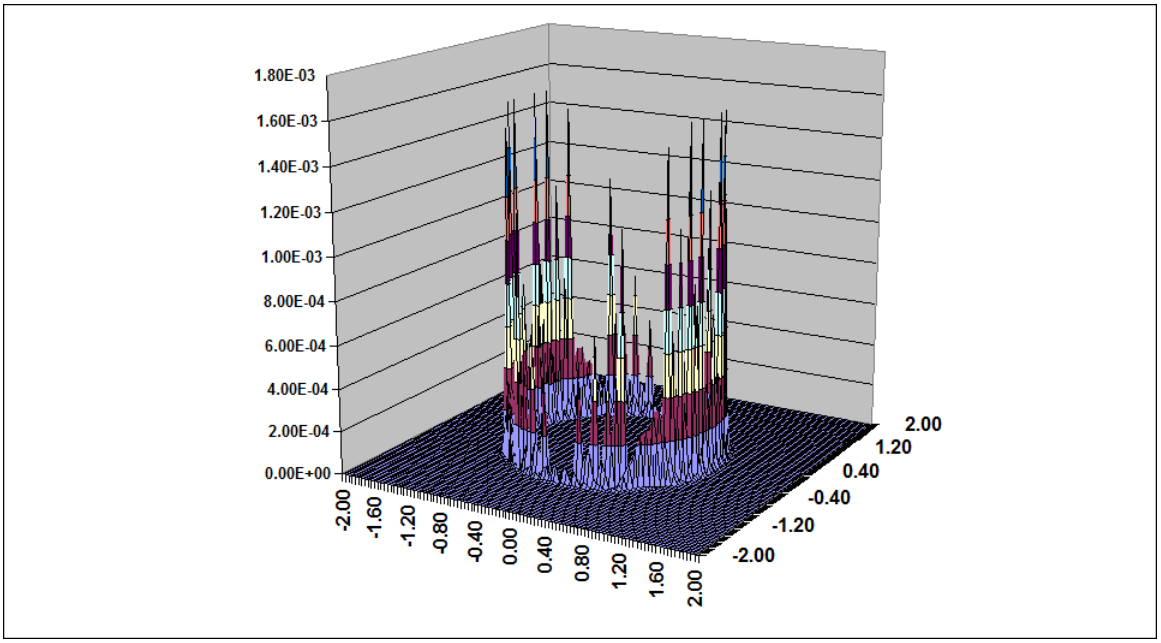

Figure 8: Graph of absolute errors - difference between analytic and refined numerical solution

4.1.4 L2 norm error

When measuring the average global error of the numerical solution v_M on the boundary, we will use the L_2 norm on $v(\theta_i) - v_{2N}(\theta_i)$ for 10,000 points on Γ_a. This should give us an indication of the speed of convergence of the solution as we increase N.

The formulation for the L2 error is:

$$\begin{aligned} E_{2N} &= \frac{1}{\sqrt{10000}} \left\| v(\theta) - v_{2N}(\theta) \right\|_2 \\ &= \frac{1}{\sqrt{10000}} \left\{ [v(\theta_1) - v_{2N}(\theta_1)]^2 + [v(\theta_2) - v_{2N}(\theta_2)]^2 + ... + [v(\theta_{10000}) - v_{2N}(\theta_{10000})]^2 \right\}^{\frac{1}{2}}. \end{aligned} \tag{90}$$

Table 2 shows the average global error for values of v on the boundary Γ_a using different number of sample points, M.

M	L_2 error
4	1.836 x 10^{-9}
8	2.210 x 10^{-9}
16	2.355 x 10^{-9}
32	2.473 x 10^{-9}
64	2.643 x 10^{-9}
128	2.932 x 10^{-9}

Table 2: L2 error for v on the boundary Γ_a

Table 3 shows the average global error for values of v in the domain D, and is the absolute difference between the analytic and numerical solutions. A square grid of points is generated in this case using 100×100 points in the (x, y)-region [-5,5]×[-5,5], and the average L_2 norm is calculated on these 10,000 points using different values of M. The outlying error values in the vicinity of the pipe boundary are excluded (we ignore values of v when $\epsilon \leq \frac{a}{10}$). It can be seen from these results that the rate of convergence is exponential up to 64 points at which point the error is most likely due to computer precision errors and is of the same order of magnitude as the error in the values on the boundary itself.

M	L_2 error
4	3.553 x 10^{-2}
8	5.671 x 10^{-3}
16	4.402 x 10^{-4}
32	5.257 x 10^{-6}
64	2.752 x 10^{-9}
128	2.588 x 10^{-9}

Table 3: L2 error for grid of values v in D

4.2 Exterior Neumann problem on a semi-infinite domain

In example §4.1, as the pipe was deep underground, we ignored the boundary condition at ground level since this had negligible effect on the solution. In this example we still want to compare our numerical results with the analytic solution, so we set $Y = 2$ and set the boundary values on the line $y = Y$ to be:

$$v = \frac{a^2 \cos\theta(x, Y)}{r(x, Y)}.$$

We can easily re-express this in Cartesian terms so that:

$$\begin{aligned} v(x, Y) &= \frac{a^2 x}{(x^2 + Y^2)} \\ \left.\frac{\partial v}{\partial y}\right|_{y=Y} &= \frac{-2a^2 xY}{(x^2 + Y^2)^2}. \end{aligned} \tag{91}$$

We do not expect discontinuous solutions on the boundary $y = Y$, since integrating both the Green's function at the load point and at the reflected point ensure there is no jump discontinuity when $p \in \Gamma_1$. We should also note that this is a well-posed problem since the compatability condition is satisfied. In fact, $\tilde{g}$ is an odd function so will always integrate to 0 over the real line.

This example will therefore test that our formulation for all operators A,B and C is correct and give confidence that we can solve any exterior problem with good accuracy (away from the vicinity of the pipe boundary).

4.2.1 Numerical Solution

The following graph is a surface plot of the solution v in the box [-2,2]×[-2,2] so that the upper boundary is ground level. Note that the plot looks extremely similar to the previous example which is as we would expect given the contrived boundary condition at y=Y. We will also initially run this without the refinements around the boundary to see if we get similar results.

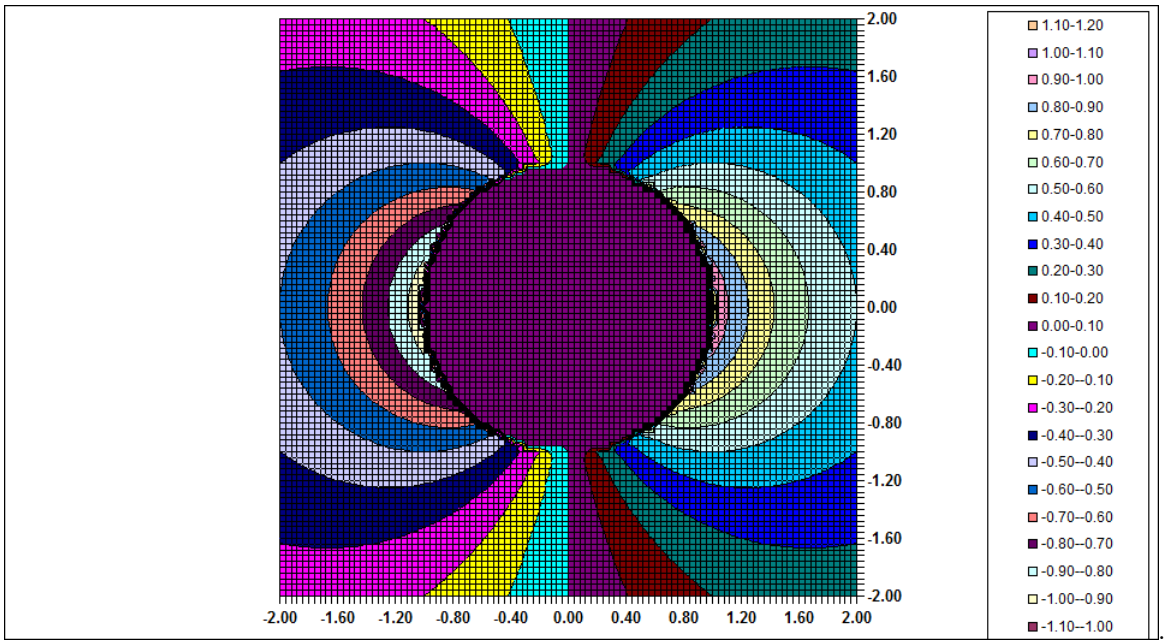

Figure 9: Graph of numerical solution with Y=2.0

4.2.2 Global Error Observations

Next we plot the global error between the analytic solution from the example §4.1 and the numerical solution. The first graph shows errors without refinement near the boundary, the second includes the refinement. As with the previous example, a considerable error reduction is observed.

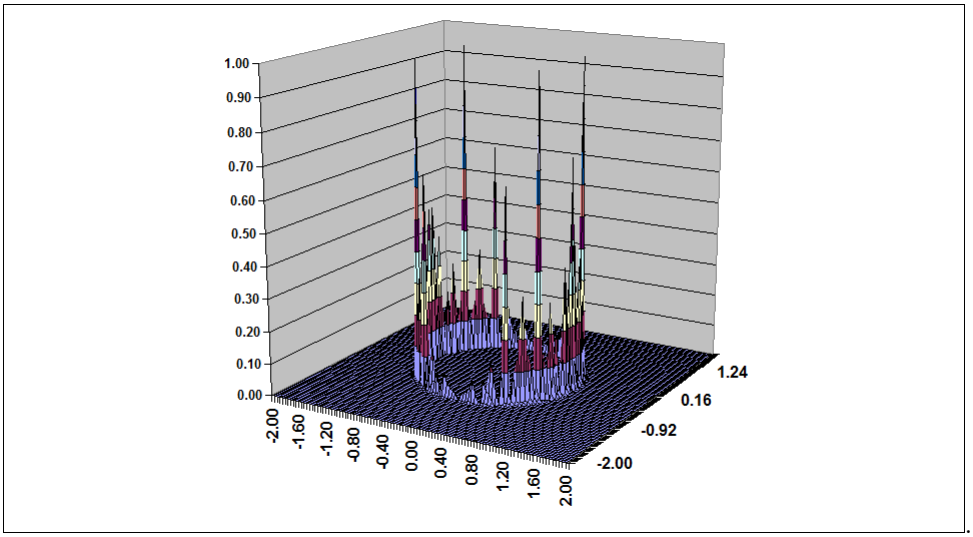

Figure 10: Absolute errors between analytic and numerical solution with Y=2.0

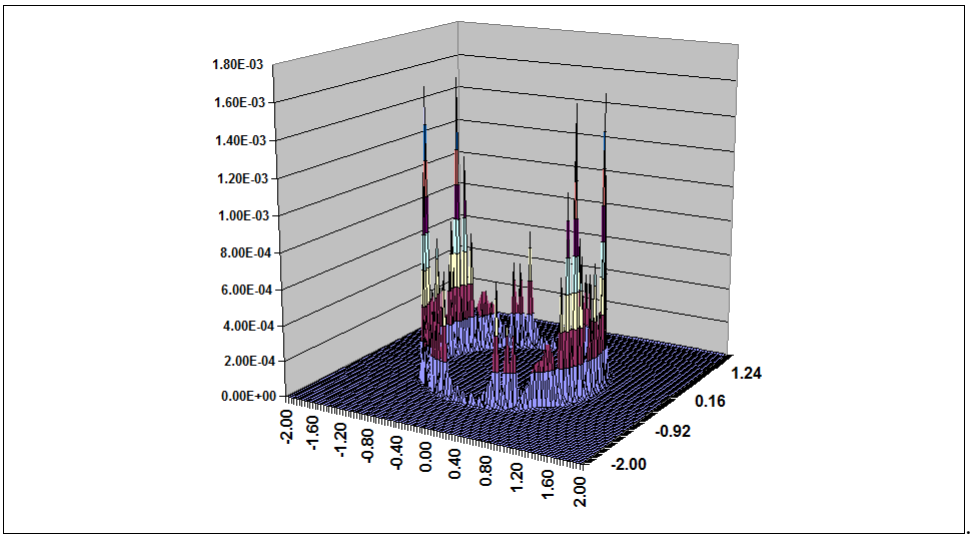

Figure 11: Absolute errors between analytic and refined numerical solution with Y=2.0

4.2.3 L2 norm error

Table 4 shows the average global error for values of v on Γ_a using different numbers of sample points. Again this shows better than exponential convergence in the solution to 32 points at which point numerical precision dominates the error term.

M	L_2 error
4	8.829 x 10^{-3}
8	1.172 x 10^{-4}
16	1.420 x 10^{-8}
32	9.316 x 10^{-10}
64	1.310 x 10^{-9}
128	1.823 x 10^{-9}

Table 4: L2 error for v on the boundary Γ_a

Table 5 shows the average global error for values of v in the domain D. A square grid of points is generated in this case using 100×100 in the (x, y)-region [-2,2]×[-2,2] and the average L_2 norm is again calculated on these 10,000 points using different values of N. The outlying error values on the pipe boundary are excluded in order to ascertain the rate of convergence in the region where the solution is well-behaved. In addition, we have also excluded the points that lie on the line $y = Y$ since these values are subject to small errors caused by the integration over Γ_1 where there is a singularity in $\tilde{G}$. These errors tend to dominate the L2 norm error and hence cloud any trend in the convergence rate elsewhere in the domain.

We can see that rate of convergence is nearly exponential up to $M = 64$ but at which point, errors

in the integration across Γ_1 dominate since this is dependent on how many sample points we use on the top boundary and is independent of M.

M	L_2 error
4	8.433 x 10^{-2}
8	1.375 x 10^{-2}
16	1.074 x 10^{-3}
32	1.407 x 10^{-5}
64	1.949 x 10^{-6}
128	1.949 x 10^{-6}

Table 5: L2 errors for a grid of values v in D

4.3 Exterior Neumann problem on semi-infinite region with non-zero c

In this example, we introduce a non-zero c term which has an interesting effect on the solution v near the pipe boundary. As described in §1, $u \to cy + T_0$ far away from the pipe. As temperature increases for large negative y, c must have a negative value. The variable v is independent of c, but it does affect the boundary condition $\tilde{f} = f + c\sin\theta$. $\tilde{g}$ is also independent of c, since $\dfrac{\partial u}{\partial y}$ and hence $g \to c$ as $|x| \to \infty$.

For this example, we are considering $f = \cos\theta$. (A trigonometric condition is sensible since it has to be 2π-periodic). Therefore in this case:

$$\begin{aligned}\tilde{f} &= f + c\sin\theta \\ &= \sqrt{1+c^2}\left(\frac{\cos\theta}{\sqrt{1+c^2}} + c\frac{\sin\theta}{\sqrt{1+c^2}}\right) \\ &= \sqrt{1+c^2}\cos(\theta + \cos^{-1}\frac{1}{\sqrt{1+c^2}}).\end{aligned} \tag{92}$$

Hence the normal derivative has undergone a rotation of $\cos^{-1}\frac{1}{\sqrt{1+c^2}}$, and has been scaled up by $\sqrt{1+c^2}$.

4.3.1 Numerical Solutions

We illustrate this rotation and scaling in Figures 12–14 and also demonstrate convergence for a different number of sample points, M. We have used the same parameters as example §4.2, except that $c < 0$ and the boundary condition $\tilde{g} = xe^{-x^2}$. Again, this function is odd and therefore integrates to 0 over the real line.

Firstly, we show a plot using $c = -0.5$ and $M = 16$. For this number of sample points, we can observe a lack of convergence particularly around the pipe boundary. There is already a discernible rotation of the solution compared to example §4.2 at this point.

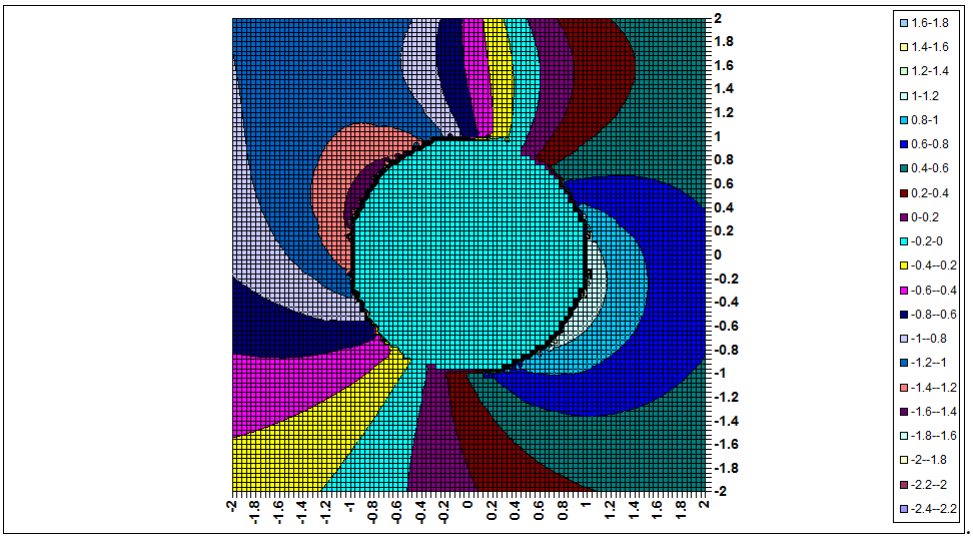

Figure 12: Graph of numerical solution - $Y = 2.0, c = -0.5, M = 16$

Next, we show the solution using $M = 64$. Here convergence has already taken place away from the pipe boundary and we can start to see that the solution has a similar pattern to example §4.2.

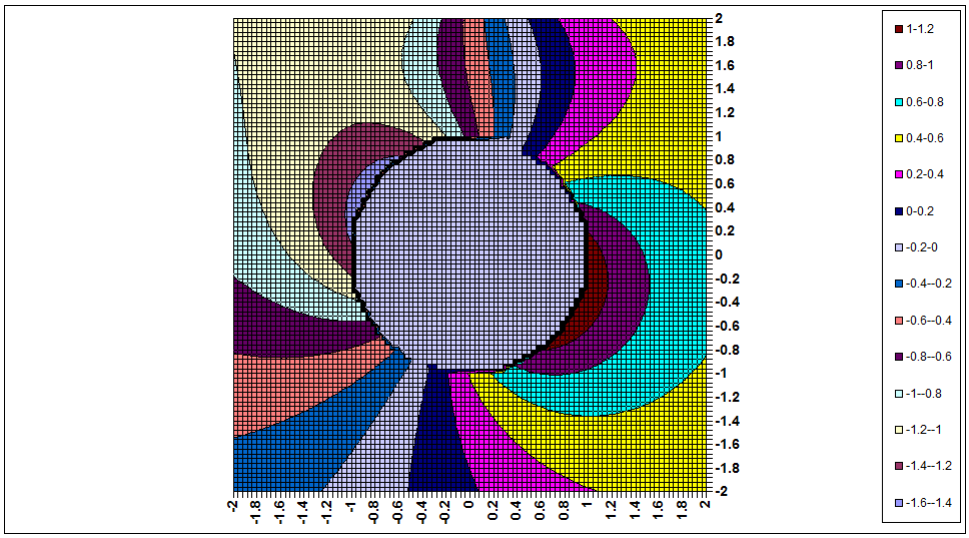

Figure 13: Graph of numerical solution - $Y = 2.0, c = -0.5, M = 64$

In Figure14, we are using $M = 256$. Given that convergence is established we will use this to be our "true" solution. Here we can see clearly that the solution, particularly around the pipe boundary, has been rotated by approximately $\frac{\pi}{6}$ compared to the solution in example §4.2. The magnitude of the solution near the boundary is also larger - we would intuitively expect this since the solution still has to decay to zero for large values of x, y but we start with a larger normal derivative on the boundary.

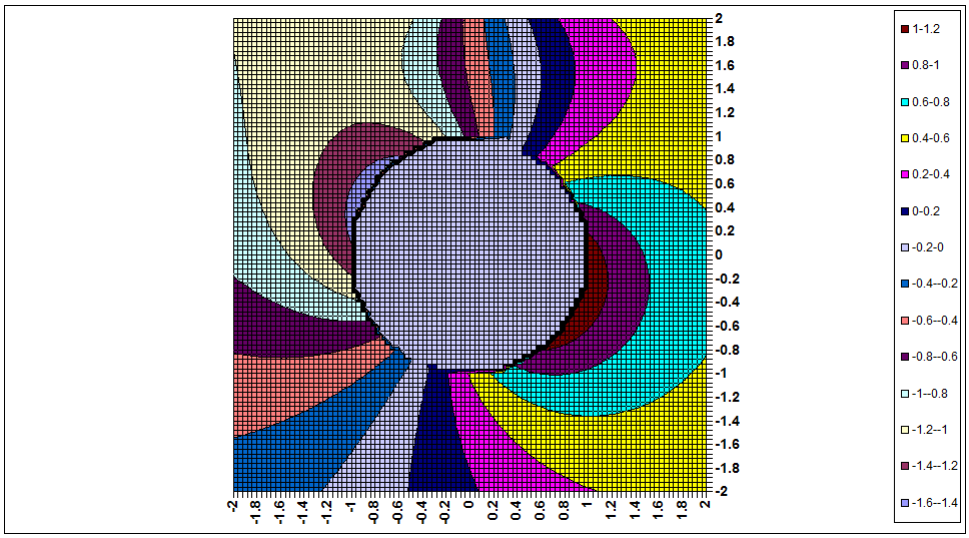

Figure 14: Graph of true numerical solution - $Y = 2.0, c = -0.5, M = 256$

Finally, we illustrate in Figure 15 the feature of rotation for a different value $c = -1$. Here we would expect a rotation of $\frac{\pi}{4}$ and a scaling factor of $\sqrt{2}$ on the normal derivative versus the solution in example 4.2.

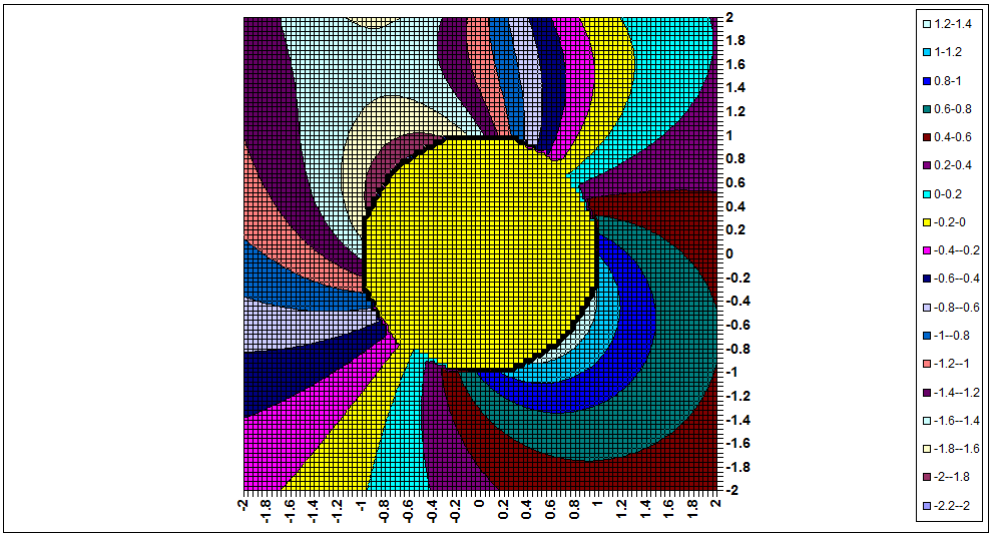

Figure 15: Graph of "true" numerical solution - $Y = 2.0, c = -1.0, M = 256$

Even though we have no analytic solution to compare to, we can still sense check some of the results. Clearly we can laboriously check that $\nabla^2 v = 0$ by using the five point formula that we used for Finite Differences Method in §1. Additionally we can check that the numerical solution satisfies the boundary conditions. Using the last example, we can evaluate $\frac{\partial v}{\partial n}, \frac{\partial^2 v}{\partial n^2}, \frac{\partial^3 v}{\partial n^3}$ using the nearest five points to the boundary $y = Y$. Using Taylor's theorem, we can then get a numerical approximation for $\frac{\partial v}{\partial n}$ on the

boundary and compare it to the value given by the boundary condition. For the last example, the largest discrepancy using such a method was 2.0042×10^{-4}. This gives us confidence that the model is converging to the correct values.

4.3.2 Global Error Observations

Figure 16 shows us the error between the two runs with 64 and 256 sample points. Again it clearly demonstrates convergence away from the pipe boundary and implies that relatively few sample points are needed for a convergent solution for a sparse grid of points in the domain, whilst if the focus is on accuracy around the pipe boundary then we need a larger number of sample points.

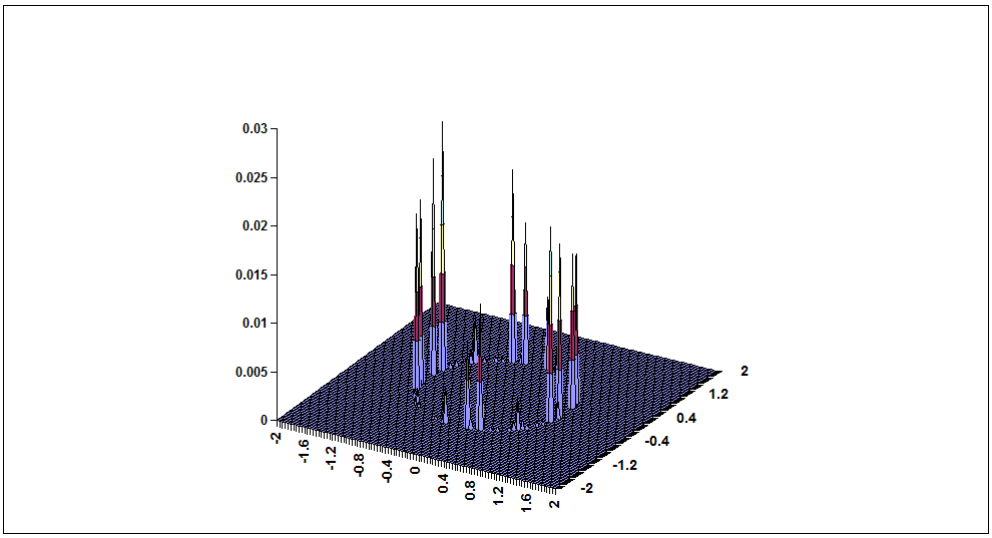

Figure 16: Absolute error - difference between numerical solutions with 64 and 256 sample points

4.3.3 L2 norm error

Table 6 shows the average global error for values of v on the boundary Γ_a using different numbers of sample points. Again this shows exponential convergence in the solution to 32 points at which point numerical precision dominates the error term.

M	L_2 error
4	5.852×10^{-2}
8	4.793×10^{-3}
16	2.223×10^{-5}
32	2.716×10^{-9}
64	2.630×10^{-9}
128	2.318×10^{-9}

Table 6: L2 error of v on boundary Γ_a

Table 7 shows the average global error for values of v in the domain D. A square grid is generated in this case using 100×100 points in the (x, y)-region [-2,2]×[-2,2] and the average L_2 norm is again calculated on these 10,000 points using different values of M. The outlying error values on the pipe boundary are again excluded as described above. If we include the discontinuity errors then the global error appears fairly constant for all M. We can see that rate of convergence is nearly exponential upto $M = 64$ but at which point, errors in the integration across Γ_1 dominate since this is dependent on how many sample points we use on the top boundary and is independent of M.

M	L_2 error
4	1.328 x 10^{-1}
8	2.023 x 10^{-2}
16	1.586 x 10^{-3}
32	2.067 x 10^{-5}
64	5.896 x 10^{-9}
128	2.800 x 10^{-12}

Table 7: L2 errors for a grid of values v in D

4.4 Successive Examples as pipe approaches ground level

Here we look to see what happens to our solution as the pipe moves from being deep underground to near ground level. In mathematical terms, we will run the simuluation from Y = 1.5, 1.25, 1.04 and 1.0 to examine if there is any breakdown in the convergence of the solution (at $Y = 1.0$, the top of the pipe is at ground surface level). This might be expected since, unlike before, the derivative of the reflected Green's function integrated round the pipe boundary becomes singular for load points $\mathbf{p} \in \Gamma_1$. In order to get a good comparison with the previous convergent results, we will again use:

- $c = 0$
- $\tilde{f} = \cos\theta = \dfrac{x}{a}$
- $\tilde{g} = \dfrac{-2xY}{(x^2 + Y^2)^2}$
- $M = 64$.

We will also use the refinements to the solution around the pipe boundary to optimise accuracy, along with the observation that if $\mathbf{p}$ is the point $(0, Y)$ then any integrals involving the reflected Green's function/Fundamental Solution (or its derivative) are the same as those using the Fundamental Solution itself. Whilst this prevents blow up at the exact singularity point, we would still expect increasing error as the load point $\mathbf{p}$ approaches the line $y = Y$.

The next page displays graphically how the solution behaves, but it is also useful to analyse the L2 error for numerical solutions derived on the line $y = Y$ versus the analytic solution. In this example we have solved for a grid of solutions in the box [-2,2]×[Y-4,Y] with $\Delta x = \Delta y = 0.04$. This gives us

101×101 grid of solutions. The reason for including $Y = 1.04$ as one of our simulations is that solutions on $y = 1.00$ give us the closest comparison (one grid spacing difference) to our solution for $Y = 1.00$ without the solution being singular on that line.

The results of the L2 errors are shown in Table 8:

Y	L_2 error
1.50	1.3907 x 10^{-6}
1.25	1.8891 x 10^{-6}
1.04	4.9068 x 10^{-5}
1.00	4.8857 x 10^{-3}

Table 8: L2 errors for differing values of Y

On closer inspection of the raw data, the solution appears to break down on the final simulation, in the region where $x \in$[-0.25,+0.25]. This does imply that it is not only at the singularity point where there is significant error but in the region close to it also. However, looking at the results in Table 8, we still get relatively good convergence for the case where $Y = 1.04$. Therefore, one approach to reduce the error when $Y = 1.00$ might be to run simulations with $Y = 1.08$ and 1.04 and then linearly extrapolate a solution for $Y = 1.00$.

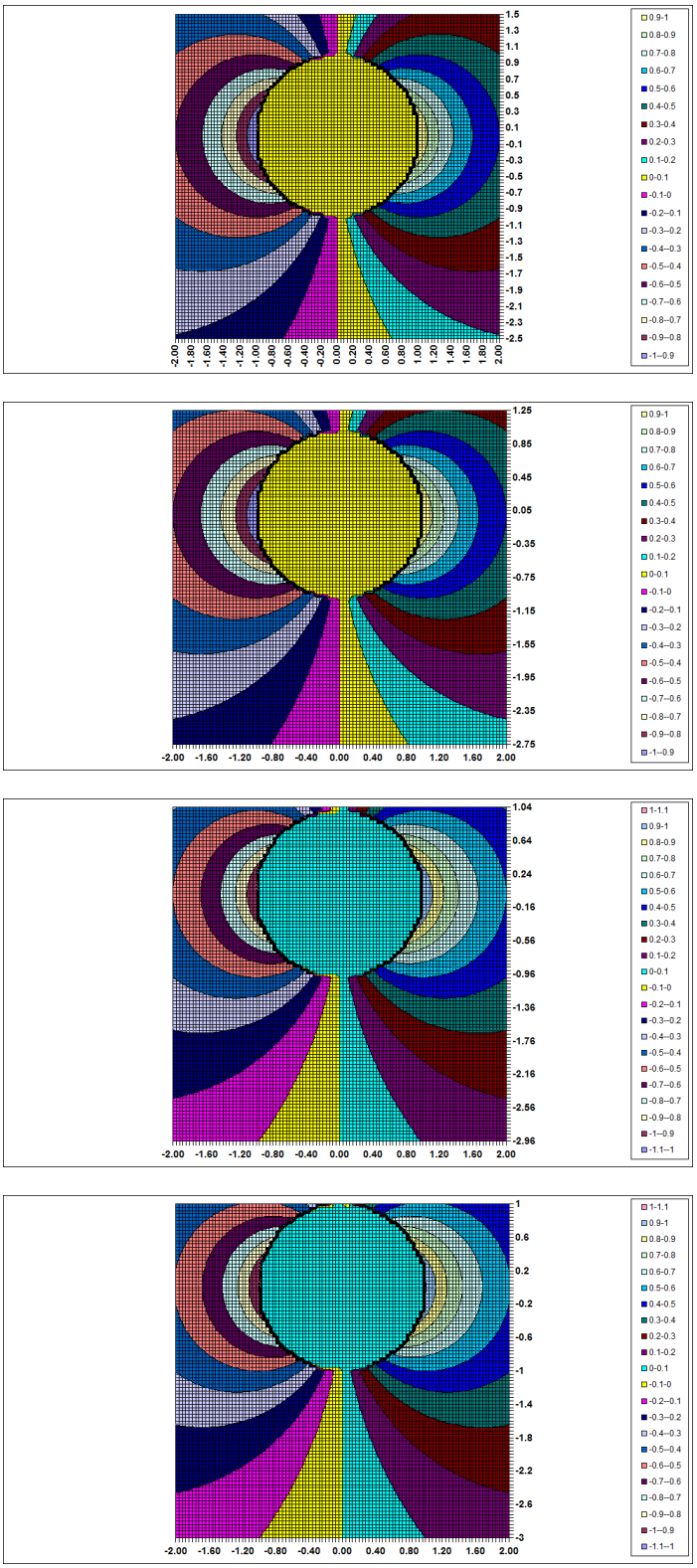

Figure 17: Evolution of numerical solution for $Y = 1.5, 1.25, 1.04, 1.0$

5 Partially Buried Pipe

In this section, we now look to reformulate our equations to deal with the situation where the pipe is only partially submerged underground. Firstly, we will need to redefine our domains and boundaries and then also make sure that we can reapply Green's Second Identity on these new domains. Once this has been established, we will then revisit our previous examples to see what effect the emergence of the pipe has on the solution in the domain.

5.1 Background

For the pipe to be only partially submerged underground, the condition $-a < Y < a$ must hold. If $Y \geq a$, then the pipe is fully submerged and we can use our previous method. If $Y \leq -a$, then the pipe is wholly above ground, and the problem reduces to one over a semi-infinite region where the pipe has no relation to the problem.

In terms of our definitions, the main differences are:

- D_a is the interior of the circle centred at the origin with radius a. This bottom part of this region is underground, the top part above ground.
- Γ_a is the circular arc that connects the two points of the circle D_a that intersect with the line $y = Y$. These two points are $\mathbf{p_1}, \mathbf{p_2}$.
- $\mathbf{p_1} = (-\sqrt{a^2 - Y^2}, Y)$ and $\mathbf{p_2} = (+\sqrt{a^2 - Y^2}, Y)$.
- Γ_1 is now defined on the line $y = Y$ but is split into two parts. The first part runs from $(-\infty, Y)$ to $\mathbf{p_1}$, the second runs from $\mathbf{p_2}$ to $(+\infty, Y)$.
- Our domain D, contains all points $\mathbf{p}$ where $y < Y$ and $\mathbf{p} \notin D_a$.

These definitions are illustrated in Figure 18.

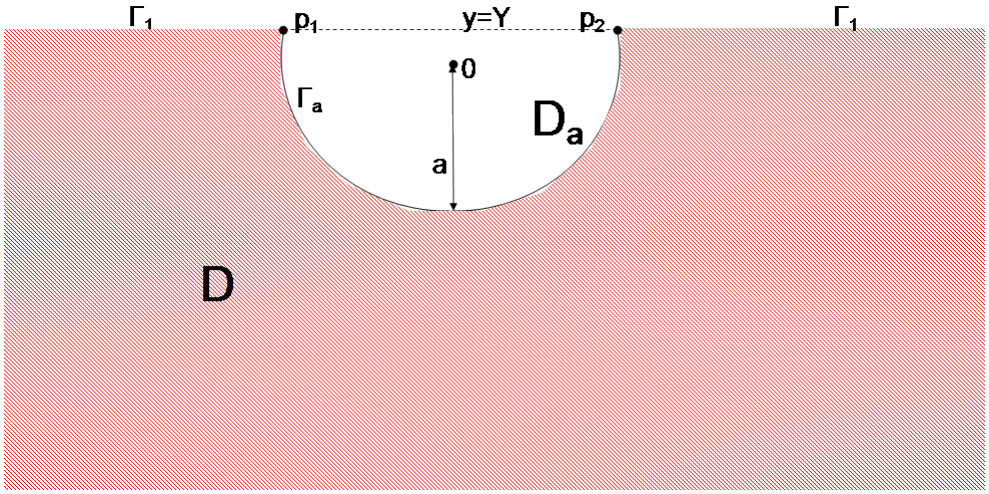

Figure 18: Layout for the partially buried pipe

5.2 Formulating the BIE

For the existence of a convergent solution we still need to stipulate that:

- $v \to 0$ as $x \to \pm\infty$.
- $\dfrac{\partial v}{\partial n}$ must be $O(x^{-1-\alpha})$ for some $\alpha > 0$.
- The compatability condition (14) must still hold for $\tilde{f}$ and $\tilde{g}$.
- We are still solving for v over Γ_a, and using this boundary solution to solve for all points in the domain D.

There immediately appears to be a problem in defining the normal derivative $\dfrac{\partial v}{\partial n}$ at points $\mathbf{p_1}$ and $\mathbf{p_2}$, since at this intersection point the boundary has a discontinuous derivative. Given that there is also a discontinuity in the solution at the pipe boundary we may have to consider how we discretise the problem as we approach both Γ_a and Γ_1.

Using the new definitions, we can apply Green's Identity as before on the domain D.

For $\mathbf{p} \in D$:

$$v(\mathbf{p}) = \int_{\Gamma_a} \left(\frac{\partial \tilde{G}}{\partial n_q}(\mathbf{p}, \mathbf{q}) v(\mathbf{q}) - \tilde{G}(\mathbf{p}, \mathbf{q}) \tilde{f}(\mathbf{q}) \right) ds_q - \int_{\Gamma_1} \tilde{G}(\mathbf{p}, \mathbf{q}) \tilde{g}(\mathbf{q}) ds_q. \tag{93}$$

For $\mathbf{p}^* \in \Gamma_a$:

$$\frac{v(\mathbf{p}^*)}{2} - \int_{\Gamma_a} \frac{\partial \tilde{G}}{\partial n_q}(\mathbf{p}^*, \mathbf{q}) v(\mathbf{q}) = - \int_{\Gamma_a} \tilde{G}(\mathbf{p}^*, \mathbf{q}) \tilde{f}(\mathbf{q}) ds_q - \int_{\Gamma_1} \tilde{G}(\mathbf{p}^*, \mathbf{q}) \tilde{g}(\mathbf{q}) ds_q. \tag{94}$$

Thus to solve (94), we must integrate round Γ_a from points $\mathbf{p_1}$ to $\mathbf{p_2}$, and similarly for Γ_1 we must use quadrature along the line $y = Y$, omitting the interval $[-\sqrt{a^2 - Y^2}, +\sqrt{a^2 - Y^2}]$.

5.2.1 Numerical integration using mollifiers

Turning our attention initially to the right hand side (RHS) of (94), numerically this is equivalent to integrating around the whole pipe boundary and along the whole real line, and setting the functions $\tilde{f}, \tilde{g}$ to zero where the range of integration needs to be omitted. The only extra stipulation for the composite trapezium rule to work is that the function $\tilde{f} \in C^\infty$, so that the discontinuities across points $\mathbf{p_1}$ and $\mathbf{p_2}$ are smoothed out. Since we are using Gaussian quadrature to integrate across the real line, this condition need not apply to $\tilde{g}$.

Let the modified function be f^*, so that $f^*(\theta) = \tilde{f}(\theta)\eta(\theta)$. We choose $\eta(\theta)$ in such a way that:

- $f^* = \tilde{f}$ for all collocation points on the pipe boundary where $y_q \leq Y$

- $f^* = 0$ for all collocation points where $y_q > Y$.

We also need to ensure that $\eta \in C^\infty$, and that all derivatives of f^* and $\tilde{f}$ are equal at points $\mathbf{p_1}, \mathbf{p_2}$. This is equivalent to stipulating that all derivatives of η are zero at points $\mathbf{p_1}, \mathbf{p_2}$.

In obtaining our function η we can borrow an idea from Probability theory which makes use of the Cumulative Normal Distribution Function, N(x), where:

$$N(x) = \int_{-\infty}^{x} \frac{1}{\sqrt{2\pi}} e^{-\frac{1}{2}z^2} dz.$$

We see immediately that $N(-\infty) = 0$ and $N(\infty) = 1$.
The derivatives of N are:

$$\begin{aligned} N^{'}(x) &= \frac{1}{\sqrt{2\pi}} e^{-\frac{1}{2}x^2} \\ N^{''}(x) &= \frac{-x}{\sqrt{2\pi}} e^{-\frac{1}{2}x^2} \\ N^{'''}(x) &= \frac{x^2 - 1}{\sqrt{2\pi}} e^{-\frac{1}{2}x^2} \end{aligned} \tag{95}$$

and so on, so that $N^m(x) = P(x)e^{-\frac{1}{2}x^2}$, where P(x) is an $(m-1)^{th}$ order polynomial; this ensures that as $x \to \pm\infty$, $N^m(x) \to 0$.

If θ_1 and θ_2 correspond to the points $\mathbf{p_1}, \mathbf{p_2}$, and $\Delta\theta$ is some arbitrarily small interval, we need to construct η such that:

$$\begin{aligned} \eta(\theta_1) &= 1 \\ \eta(\theta_1 + \Delta\theta) &= 0 \\ \eta(\theta_2 - \Delta\theta) &= 0 \\ \eta(\theta_2) &= 1. \end{aligned} \tag{96}$$

One function that satisfies these conditions is:

$$\eta(\theta) = \begin{cases} 1 & \theta \le \theta_1 \\ N\left[\tan\left(\frac{\pi}{2} - \frac{\pi}{\Delta\theta}(\theta - \theta_1)\right)\right] & \theta_1 \le \theta \le \theta_1 + \Delta\theta \\ 0 & \theta_1 + \Delta\theta \le \theta \le \theta_2 - \Delta\theta \\ N\left[\tan\left(\frac{\pi}{2} + \frac{\pi}{\Delta\theta}(\theta - \theta_2)\right)\right] & \theta_2 - \Delta\theta \le \theta \le \theta_2 \\ 1 & \theta \ge \theta_2. \end{cases}$$

This function can be termed a mollifying function as it smoothes out the discontinuities at θ_1, θ_2.
Making the substitution $x = \tan\left(\frac{\pi}{2} - \frac{\pi}{\Delta\theta}(\theta - \theta_1)\right)$ and using results from (95), we can quickly see using the chain rule that all derivatives $\eta^m(\theta)$ are zero at the points θ_1 and $\theta_1 + \Delta\theta$. We can make a similar substitution to get the same result at $\theta_2 - \Delta\theta$ and θ_2. This ensures that $\eta(\theta)$ is infinitely differentiable around the pipe boundary and so we can now apply the composite trapezium rule.

Tests show that this approximation does give reasonable accuracy for $N = 64$. However as N is increased the approximation oscillates around the convergent value. This is probably because the Fourier series required to fit the function requires many terms given the discontinuity, and as we observed before N must be greater than the order of the Fourier series to obtain super-algebraic convergence.

5.2.2 Numerical integration using grading

- **Operators A,B**

  Another more obvious approach is to integrate around the circle from θ_1 to θ_2 using Gaussian quadrature with grading. When we were integrating round a full circle we were able to isolate the singularity using the properties of the Lagrangian basis functions. However, we now know that for $\mathbf{p}* \in \Gamma_a$ there will be a singularity in the integrand.

  Supposing this singularity occurs when $\theta = \theta^*$, then we should perform Gaussian quadrature with grading from θ_1 to θ^* and also from θ^* to θ_2. Using 8 points for each graded domain should ensure better convergence than for 64 points with no grading.

- **Operator C**

  When integrating operator C, we may also need to refine our methodology since if we simply make $g(\tilde{x}) = 0$ in the range $[x_1, x_2] = [a\cos\theta_1, a\cos\theta_2]$, then $\dfrac{\partial g}{\partial x}$ becomes infinite across the discontinuity which will effect convergence of the integral. An alternative approach follows.

  Suppose $\mathbf{p} \in D$ is sufficiently far away from Γ_1. Therefore the kernel of operator C will not be singular. We only need to split the integral into two parts:

$$(C\tilde{g})(\mathbf{p}) = \int_{-\infty}^{-x_2} \tilde{G}(x_q)\tilde{g}(x_q)dx_q + \int_{x_2}^{\infty} \tilde{G}(x_q)\tilde{g}(x_q)dx_q \quad = \int_{x_2}^{\infty} \left(\tilde{G}(x_q)\tilde{g}(x_q) + \tilde{G}(-x_q)\tilde{g}(-x_q)\right) dx_q. \tag{97}$$

  As the integrand is not singular, this can be integrated without grading using 64 points and the $\tan^2\phi$ substitution.

  Now suppose $\mathbf{p}^* \in \Gamma_a$ given by (x_p, Y). The integral will certainly be singular at $x = x_p$. This time

we can split the integral into several regions resulting in the following integrals:

$$
\begin{aligned}
(C\tilde{g})(\mathbf{p}) &= \int_{-\infty}^{-|x_p|} \tilde{G}(x_q)\tilde{g}(x_q)dx_q + \int_{-|x_p|}^{-x_2} \tilde{G}(x_q)\tilde{g}(x_q)dx_q + \\
&\quad \int_{x_2}^{|x_p|} \tilde{G}(x_q)\tilde{g}(x_q)dx_q + \int_{|x_p|}^{\infty} \tilde{G}(x_q)\tilde{g}(x_q)dx_q \\
&= \int_{x_2}^{|x_p|} \left(\tilde{G}(x_q)\tilde{g}(x_q) + \tilde{G}(-x_q)\tilde{g}(-x_q)\right) dx_q + \int_{|x_p|}^{\infty} \left(\tilde{G}(x_q)\tilde{g}(x_q) + \tilde{G}(-x_q)\tilde{g}(-x_q)\right) dx_q.
\end{aligned}
\tag{98}
$$

These two integrals each have a singularity at $|x_p|$ so we can use grading with 8 points on 8 domains using the $\tan^2\phi$ substitution where necessary to obtain optimal accuracy.

5.3 Examples with partially buried pipe

5.3.1 Benchmark example - half buried pipe

We now illustrate the two methods described previously with an example. In order to compare against an exact analytic solution we will examine a half buried pipe where $Y = 0$. The boundary conditions are:

$$
\begin{aligned}
\tilde{f}(\theta) &= \cos\theta \\
\tilde{g}(x) &= 0.
\end{aligned}
$$

This again yields the closed-form solution $v = \dfrac{\cos\theta}{r}$.

The numerical solution evaluated by Gaussian quadrature with grading does take longer to calculate than for the fully buried pipe, so we will look at a coarser grid of 41×41 solutions over the region [-2,2]×[-4,0]. To benchmark the solution, we will show in Table 9 the L2 error (the difference between the numerical and analytic solution) over all points, and the time taken to calculate solutions for both methods using different values of M.

M	Mollifier used	L_2 error	Calculation time (secs)
64	YES	2.2220 x 10^{-4}	4
256	YES	5.2505 x 10^{-5}	32
64	NO	3.8528 x 10^{-5}	100
256	NO	2.4748 x 10^{-6}	460

Table 9: L2 error using mollifiers and graded Gaussian quadrature

On the face of it, we appear to achieve almost the same accuracy using mollifiers with 256 sample points as using graded quadrature with 64 sample points. The mollifier approach takes significantly less time to compute even with 256 points. However, this does not tell the whole story. In fact, the solution on the entire circle (i.e. the numerical solution to the BIE) is not particularly accurate using mollifiers. As an illustration, Figure 19 shows the pointwise error at each collocation point as θ goes from 0 to 2π

(here we used M=64).

Note: because we use mollifiers, we still need to collocate round the entire circle even though our solution domain does not include the top half of the circle.

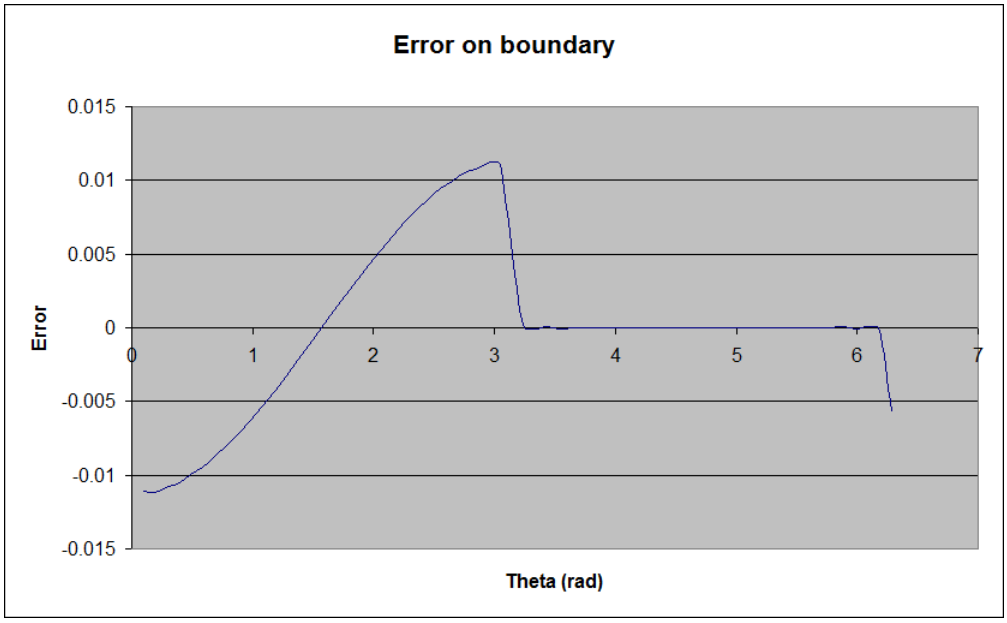

Figure 19: Difference between numerical values on pipe boundary and analytic solution

Perhaps the result is unsurprising as we are trying to use Lagrangian trigonometric functions to fit the function $\tilde{f} = 0$ for $0 \leq \theta \leq \pi$ and $\tilde{f} = \cos\theta$ for $\pi \leq \theta \leq 2\pi$.

By contrast, the pointwise error on Γ_a when using graded quadrature is of the order 10^{-10} for each collocation point. The major contributor to the L2 error on our grid of solutions is in the case where we use the Taylor's expansion. We can only get $O(\epsilon)$ accuracy here because $v_{\theta\theta} = 0$ using piecewise constant interpolation. The implication here is that for points far away from the pipe boundary, the mollifier method will give quick and reasonably accurate solutions. For more precision close to the pipe boundary we should use graded quadrature.

5.3.2 Successive examples as pipe emerges above ground

Our benchmark example above used a particular boundary condition $\tilde{g} = 0$ to allow us to compare with the analytic solution. We now examine a series of solutions using $Y = 0.50, 0.00, -0.50, -0.90$ where $\tilde{g}(x)$ does not depend on Y. To satisfy the compatability condition and keep some continuity with previous examples we will use $\tilde{f}(\theta) = \cos\theta, \tilde{g}(x) = xe^{-x^2}$.

This does not have a simple analytic solution, so our "true" solution will be that using graded quadrature and M=256. Since the most interesting region to look at is near to the boundary of the pipe we have

solved for a grid 41×41 points in the region [-1,1]×[Y-2,Y]. For each value of $Y = 0.50, 0.00, -0.50, -0.90$, we run the simulation using $M = 64$ with graded quadrature. For the case $Y = 0$, we compute the L2 error against the "true" solution (i.e. with $M = 256$) which turns out to be 2.9439×10^{-5}. This gives us confidence that our solutions using $M = 64$ will be sufficiently accurate using other values of Y. The reason for using $M = 64$ is the time saving it gives us (100 secs per run rather than 460 secs).

The results of the simulations are shown in Figure 20. We can see immediately that away from the pipe boundary, we have a convergent solution; close to the boundary it is harder to discern due to the coarseness of the grid whether the solution has converged sufficiently. Drilling down into the raw data, we can see that the numerical solution does indeed satisfy Laplace's Equation and the boundary conditions to within an acceptable tolerance which suggests that the method is robust and convergent.

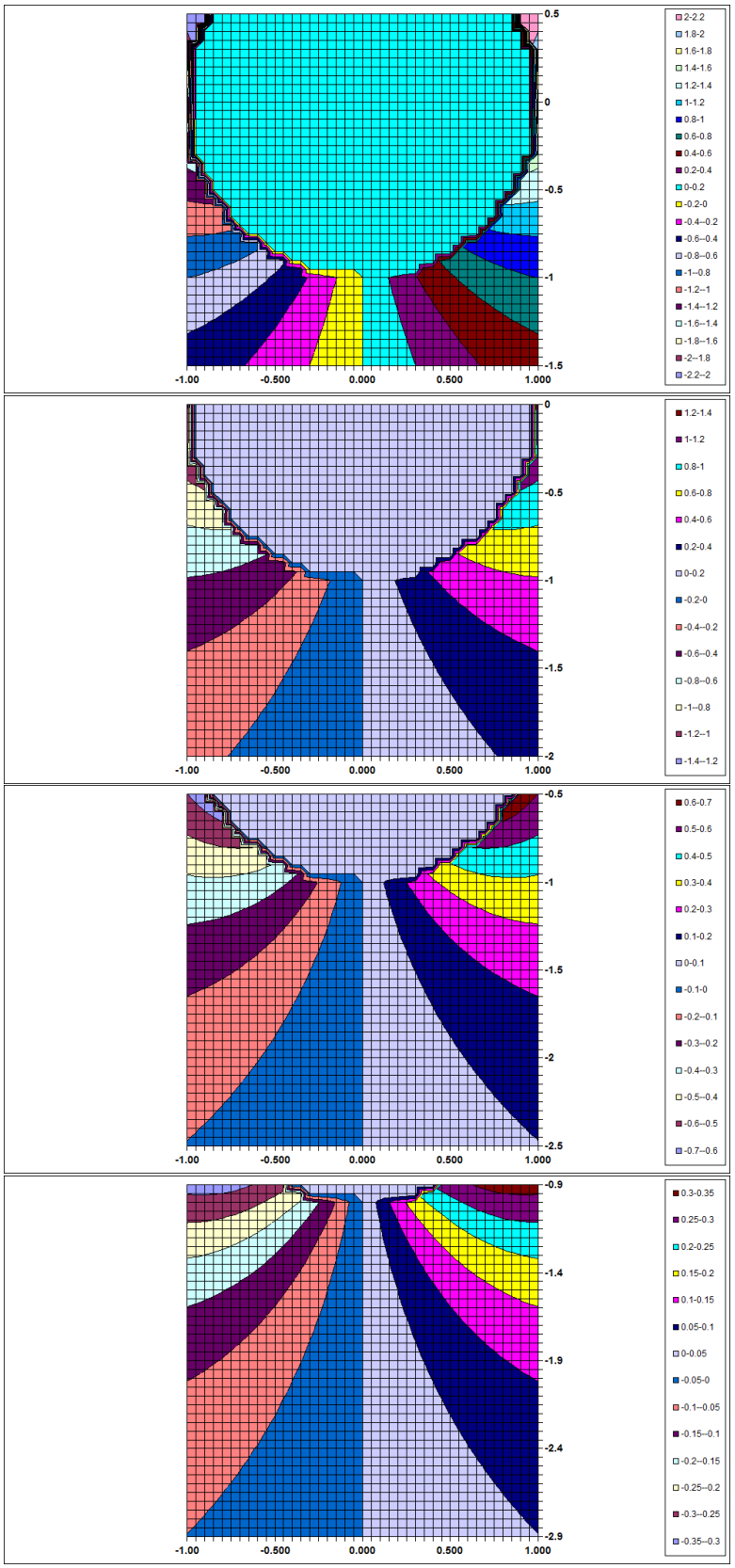

Figure 20: Evolution of solution as Y goes from +0.5 to -0.9

6 Conclusions

In this dissertation, we have demonstrated that the BEM is a very powerful technique to solve Laplace's Equation, particularly in the situation where we have an infinite or semi-infinite exterior domain and Neumann boundary conditions. By comparing our solutions to known analytic solutions with certain boundary conditions we have been able to show that away from the boundary, the numerical solution using BEM converges rapidly with a relatively small number of sample points. We have also illustrated two numerical methods, Nyström's Method and the collocation method, where a linear system of equations can easily be solved to give us our solution. In the case of the collocation method, we have highlighted the use of Lagrangian trigonometric basis functions, which lend themselves very well to circular boundaries. Not only is the interpolation of solutions on the boundary smooth, but so are all their derivatives which means that for 2π-periodic boundary functions, we can use the composite trapezium rule to numerically integrate and expect rapid (super-algebraic) convergence. These basis functions can also be of use when confronted with some singular integrals (e.g. logarithmic kernels), since we can evaluate these analytically in certain cases.

Whilst we can use these techniques to get very accurate solutions on the boundary itself, when we approach the pipe boundary, we find that the solution converges slowly. Therefore we have developed some alternative approaches. One simple approach is to increase the number of collocation points as we approach the boundary. When we are extremely close to the boundary, we can use a Taylor's expansion to get a good approximation, since we know that our solution on the boundary is accurate. We also know the first derivative of the solution since that is our Neumann condition, and we can derive an approximate second derivative from Laplace's Equation. Both these techniques improve accuracy considerably and we demonstrate this in §4.

Our original aim was to develop a model that could also handle a partially buried pipe. This requires different treatment to the entirely buried pipe because our boundary is not a full circle any more and thus many of the elegant properties of the Lagrangian basis functions do not necessarily hold. We examine two different approaches to try and circumvent these issues. The first approach is to evaluate the integrals over the buried part of the pipe, by integrating over the full circle and setting the boundary function to 0 where the pipe is above ground. To maintain infinite differentiability we need to use mollifying functions. The second approach uses a more obvious method where we use piecewise constant basis functions and Gauss-Legendre quadrature to numerically integrate over the part of the circle that is underground. Where there are singularities, we have numerically integrated using grading to minimise its effect. Both approaches are outlined in §5. Finally we run some simulations as the pipe emerges from the ground to demonstrate that the numerical method behaves as expected and does not "blow up".

We have not attempted to run any real physical simulations on this model, but have demonstrated that the model we have implemented converges well to known analytic solutions and to simulations with large number of sample points and therefore should be fit for purpose when used in an industrial environment.

References

[1] M. Abramowitz and I. Stegun: Handbook of Mathematical Functions, Dover (2006)

[2] K. Atkinson: Numerical Solutions of Integral Equations of the Second Kind, Cambridge University Press (1997)

[3] H. Bau: Cognitive Heat Losses from pipe buried in semi-infinite porous medium, International Journal of Heat and Mass Transfer, Vol 27, Issue 11, pp 2047-2056 (1984)

[4] H. Bau and S. Sadhal: Heat Losses from Fluid Flowing in a Buried Pipe, International Journal of Heat and Mass Transfer, Vol 25, Issue 11, pp 1621-1629 (1982)

[5] W. Briggs and Van Emden Henson: The DFT - an owner's manual for the discrete Fourier Transform,SIAM (1995)

[6] O. Bruno, C. Geuzaine, J. Monro, F. Reitich: Prescribed error tolerances within fixed computational times for scattering problems of arbitrarily high frequency, The Royal Society, pp 629-645 (1984)

[7] M. Chung, P. Jung and R. Rangel: Semi-analytical solution for heat transfer from a buried pipe with convection on the exposed surface, International Journal of Heat and Mass Transfer, Vol 42, pp 3771-3786 (1999)

[8] A. Dayan, A. Merbaum and I. Segal: Temporary Distributions around Buried Pipe Networks, International Journal of Heat and Mass Transfer, Vol 27, Issue 3, pp 409-417 (1984)

[9] P. DuChateau, D. Zachmann: Schaum's Outline of Partial Differential Equations (1986)

[10] S. Johnson: Notes on the convergence of Trapezoidal Rule Quadrature, http://math.mit.edu/stevenj/trapezoidal.pdf (2010)

[11] R. Kress: Linear Integral Equations - Second Edition, Springer-Verlag (1999)

[12] S. Langdon: Pers. Comm. (2010)

[13] C. Ovuworie: Partially Buried Pipe Heat Transfer Presentation (2008)

[14] C. Ovuworie: Steady-State Heat Transfer Models For Fully And Partially Buried Pipelines, Society of Petroleum Engineers (SPE) paper 131137-MS, 2010 (doi 10.2118/131137-MS)

[15] A. Sadegh, L. Jiji and S. Weinbaum: Boundary integral equation technique with application to freezing around a buried pipe, International Journal of Heat and Mass Transfer, Vol 30, Issue 2, pp 223-232 (1987)

[16] F. Scheid: Schaum's Outline of Theory and Problems of Numerical Analysis, Second Edition (1989)

[17] I. Sloan: Error Analysis of boundary integral methods, Acta Numerica, pp 287-339 (1991)

[18] Web page: http://en.wikipedia.org/wiki/Bipolar_coordinates

[19] Web page: http://en.wikipedia.org/wiki/TauTona_Mine

[20] Web page: http://en.wikipedia.org/wiki/Two-center_bipolar_coordinates

[21] Web page: http://www4.ncsu.edu/ rsmith/MA573_F09/Heat_Equation.pdf